NACA RM A52K13

MAR 2 1953

CONFIDENTIAL
SECURITY INFORMATION

NACA

RESEARCH MEMORANDUM

TESTS IN THE AMES 40- BY 80-FOOT WIND TUNNEL OF AN AIRPLANE

MODEL WITH AN ASPECT RATIO 4 TRIANGULAR WING AND AN

ALL-MOVABLE HORIZONTAL TAIL - HIGH-LIFT

DEVICES AND LATERAL CONTROLS

By Ralph W. Franks

Ames Aeronautical Laboratory
Moffett Field, Calif.

NATIONAL ADVISORY COMMITTEE
FOR AERONAUTICS

WASHINGTON

February 20, 1953

NACA RM A52K13

NATIONAL ADVISORY COMMITTEE FOR AERONAUTICS

RESEARCH MEMORANDUM

TESTS IN THE AMES 40- BY 80-FOOT WIND TUNNEL OF AN AIRPLANE

MODEL WITH AN ASPECT RATIO 4 TRIANGULAR WING AND AN

ALL-MOVABLE HORIZONTAL TAIL - HIGH-LIFT

DEVICES AND LATERAL CONTROLS

By Ralph W. Franks

SUMMARY

Tests have been made of a triangular-wing-airplane model equipped with high-lift devices and lateral and directional controls. The model consisted of an aspect ratio 4 triangular wing in combination with a fuselage of fineness ratio 12.5; a thin, triangular, vertical tail with a constant-chord rudder; and a thin, unswept, all-movable horizontal tail. The wing had an NACA 0005 modified section and was equipped with partial-span, constant-chord, slotted inboard flaps, and plain, constant-chord, outboard flaps.

Three lateral controls were tested; namely, the inboard flaps, the outboard flaps, and the all-movable horizontal tail. The high-lift devices were the outboard flaps and the inboard flaps. Tests were made with the wing-fuselage-vertical-tail configuration in addition to the tests of the complete model. The Reynolds number, based on the wing mean aerodynamic chord, was approximately 10.9 million and the Mach number was approximately 0.13.

INTRODUCTION

The low-speed aerodynamic characteristics of an airplane model with an aspect ratio 4 triangular wing and an all-movable horizontal tail have been under investigation in the Ames 40- by 80-foot wind tunnel. The longitudinal aerodynamic characteristics of the model at zero sideslip have been reported in reference 1; included therein were data covering the effect of horizontal-tail aspect ratio and vertical location. The

results of the tests of reference 1 indicated that the horizontal tail having the greater aspect ratio (4.4) located in the extended wing-chord plane gave the best stability and the lowest drag; therefore, this tail configuration was used in the present investigation.

Presented herein are the results of tests of the model with high-lift devices, and lateral and directional controls. The high-lift devices included slotted inboard flaps and plain outboard flaps. Three lateral controls were tested; namely, the inboard flaps, the outboard flaps, and the all-movable horizontal tail. In addition, a rudder of constant chord was tested as a directional control device. The data herein are presented without analysis to expedite publication.

NOTATION

The coefficients and symbols used in this report are defined as follows and as shown in figure 1, wherein all force and moment coefficients, angles, and control deflections are shown as positive. All control deflections are measured in a plane perpendicular to the control hinge line.

α angle of attack of the wing-chord plane with reference to free stream, degrees

b wing span, feet

b_i inboard flap span (total movable), feet

b_o outboard flap span (total movable), feet

b_t horizontal-tail span, feet

β angle of sideslip of the model center line with reference to free stream, degrees

c wing chord, measured parallel to wing center line, feet

$\bar{c}$ mean aerodynamic chord of wing, measured parallel to wing center line $\left(\dfrac{\int_0^{b/2} c^2 dy}{\int_0^{b/2} c\, dy} \right)$, feet

C_D drag coefficient $\left(\dfrac{\text{drag}}{qS} \right)$

C_l rolling-moment coefficient $\left(\dfrac{\text{rolling moment}}{qSb}\right)$

C_L lift coefficient $\left(\dfrac{\text{lift}}{qS}\right)$

C_m pitching-moment coefficient $\left(\dfrac{\text{pitching moment}}{qS\bar{c}}\right)$

C_n yawing-moment coefficient $\left(\dfrac{\text{yawing moment}}{qSb}\right)$

C_Y side-force coefficient $\left(\dfrac{\text{side force}}{qS}\right)$

δ_i average deflection of the inboard flaps, degrees

δ_l difference in deflection between any pair of control surfaces used as lateral controls, positive when left-hand surface has the more positive deflection, degrees

δ_o average deflection of the outboard flaps

δ_r rudder deflection (positive when trailing edge moves to left), degrees

Δ prefix denoting an increment

ϵ_{av} average effective downwash angle, degrees

i_t average horizontal-tail incidence relative to the wing-chord plane, degrees

l_t distance from moment center of model to pivot line of horizontal tail, feet

$\dfrac{L}{D}$ lift-drag ratio

p rate of rolling, radians per second

$\dfrac{pb}{2V}$ wing-tip helix angle, radians

q free-stream dynamic pressure, pounds per square foot

S wing area, square feet

S_i inboard flap area (total movable), square feet

S_o outboard flap area (total movable), square feet

S_r rudder area (total movable), square feet

S_t horizontal-tail area (total movable), square feet

V free-stream velocity, feet per second

W airplane weight, pounds

x longitudinal coordinate parallel to model center line, feet

y lateral coordinate perpendicular to plane of symmetry, feet

z vertical coordinate perpendicular to wing-chord plane, feet

C_{l_β} $\left(\dfrac{\partial C_l}{\partial \beta} \right)$

C_{l_p} $\left[\dfrac{\partial C_l}{\partial (pb/2V)} \right]$

C_{n_β} $\left(\dfrac{\partial C_n}{\partial \beta} \right)$

C_{Y_β} $\left(\dfrac{\partial C_Y}{\partial \beta} \right)$

<center>Subscripts</center>

i   inboard flaps

o   outboard flaps

t   horizontal tail

<center>MODEL</center>

The model used in the present investigation was that described in reference 1, with the addition of a rudder and inboard and outboard

trailing-edge flaps. The model was equipped with the horizontal tail of aspect ratio 4.4 described in reference 1. Dimensional data of the model are presented in figure 2 and table I. A photograph of the model as mounted in the wind tunnel is shown in figure 3.

The rudder and the outboard flaps were of constant chord and had plain radius noses. The inboard flaps were of constant chord and of the slotted type. Details of the inboard flaps and the path of travel of the inboard flaps during deflection are shown in figure 4.

TESTS AND PROCEDURE

The configurations tested are listed in table II. The flaps and the horizontal tail were tested as lateral-control surfaces by deflecting these surfaces antisymmetrically, the deflections being superposed on initial symmetrical settings. During the investigation simultaneous deflections of the inboard and outboard flaps were used to simulate the effect of full-span flaps. Tests were also made with the rudder deflected to ascertain rudder effectiveness and possible control interaction between rudder and horizontal tail when the tail was being used as a lateral control.

The data were corrected for wind-tunnel-wall effects using the theory described in reference 2. These corrections were:

$$\Delta\alpha = 0.67 \ C_L$$

$$\Delta C_D = 0.012 \ C_L{}^2$$

$$\Delta C_m = -0.014 \ C_L \ (\text{tail-on configurations only})$$

The data were also corrected for support-strut interference. No corrections were applied to the data for possible deflection of the control surfaces due to aerodynamic loads since they were believed to be negligible. The accuracy of setting of all control-surface deflections was within ±0.2°. The average Reynolds number of the tests was 10.9 million based on the mean aerodynamic chord of the wing. The dynamic pressure was approximately 25 pounds per square foot and the Mach number was approximately 0.13.

RESULTS

The basic experimental data obtained are presented in figures 5 to 13, which are indexed in table II. The moment data in all figures are

referred to a moment center located at 40.8 percent of the mean aerodynamic chord of the wing. This is the moment center for which a static margin, $-(dC_m/dC_L)_{C_L=0}$, of 0.06 would be obtained when the trailing-edge flaps and the horizontal tail are undeflected.

The effects of inboard-flap deflection and horizontal-tail incidence on the pitching-moment characteristics are shown in figure 14. The variations of the average effective downwash angle with angle of attack at the position of the horizontal tail were determined from the pitching-moment data obtained during the test and are presented in figure 15. These values were determined by making the assumption that for any given tail incidence, the intersection of the tail-on and the tail-off pitching-moment curves indicates the lift-coefficient value at which the pitching moment due to the tail is zero; hence, the average angle of flow across the tail is zero. In order to obtain points of intersection for tail incidences other than those tested, a linear variation of dC_m/di_t was assumed.

In figure 16 the increments of lift coefficient obtained experimentally on the wing-fuselage-vertical-tail configuration at $0°$ angle of attack with $40°$ inboard flap deflection and various outboard flap deflections are plotted against values obtained through application of the theory of reference 3.

The trimmed lift and drag characteristics for the model in level flight, based on a 30 pounds per square foot wing loading, are shown in figure 17. The dashed portion of the lift curve indicates a region of longitudinal instability with inboard flaps deflected. This destabilizing effect, shown in the pitching-moment curves of figure 14, is believed due to the destabilizing variation of downwash with angle of attack through this region, as indicated in figure 15 by the increasing slope of the downwash curve.

The effectiveness of the flaps and the horizontal tail as lateral controls is shown in figures 18 to 21. The increments of rolling-moment coefficient were obtained from figures 5, 6, 9, and 10 and were based on a differential lateral-control deflection of $20°$. For each lateral control tested, the effectiveness as predicted by the theory of reference 4 has been plotted.

The variations of $pb/2V$ with C_L for each lateral control is shown in figure 22. In computing these values, use was made of values of rolling-moment coefficients obtained experimentally with a $20°$ differential lateral-control surface deflection, a rudder deflection of $0°$, and the model held at $0°$ sideslip. The values of C_{l_p} were obtained from figure 13 of reference 5. It should be noted that the reason for

the rapid increase of pb/2V at high lift coefficients is due to the decrease of the damping-in-roll parameter at the higher lift coefficients.

The rudder defectiveness, based on a 10° rudder deflection with inboard flaps deflected, is shown in figure 23 as well as the effect of the use of the horizontal tail as a lateral-control device on the rudder effectiveness.

The sideslip derivatives, C_{n_β}, C_{l_β}, and C_{Y_β}, as measured near 0° of sideslip from the data plotted in figures 7 and 12, are presented in figure 24. Values are shown for the wing-fuselage-vertical-tail configuration and for the complete model with flap deflections of 0° and 40° in both cases.

Ames Aeronautical Laboratory
        National Advisory Committee for Aeronautics
                Moffett Field, Calif.

REFERENCES

1. Graham, David, and Koenig, David G.: Tests in the Ames 40- by 80-Foot Wind Tunnel of an Airplane Configuration With an Aspect Ratio 4 Triangular Wing and an All-Movable Horizontal Tail - Longitudinal Characteristics. NACA RM A51H10a, 1951.

2. Tani, Itiro, and Sanuki, Matao: The Wall Interference of a Wind Tunnel of Elliptic Cross Section. NACA TM 1075, 1944.

3. DeYoung, John: Theoretical Symmetric Span Loading Due to Flap Deflection for Wings of Arbitrary Plan Form at Subsonic Speeds. NACA TN 2278, 1951.

4. DeYoung, John: Theoretical Antisymmetric Span Loading for Wings of Arbitrary Plan Form at Subsonic Speeds. NACA TN 2140, 1950.

5. Jaquet, Byron M., and Brewer, Jack D.: Low-Speed Static-Stability and Rolling Characteristics of Low-Aspect-Ratio Wings of Triangular and Modified Triangular Plan Forms. NACA RM L8L29, 1949.

TABLE I.- DIMENSIONAL DATA

Wing

Area, square feet 312.5
Span, feet 35.36
Mean aerodynamic chord, feet 11.78
Chord at fuselage center line, feet 17.68
Aspect ratio 4.0
Taper ratio 0
Airfoil section parallel to model
    center line . . . . NACA 0005 (modified)

Slotted, inboard flaps

S_i/S 0.120
b_i/b 0.539
Flap chord, percent wing chord at fuselage center line . . . 11.1

Outboard flaps

S_o/S 0.059
b_o/b 0.334
Outboard flap chord, percent wing chord at fuselage
    center line 10.5

Fuselage

Length, feet 56.16
Maximum diameter, feet 4.49
Fineness ratio 12.50

Vertical tail

S_t/S 0.168
S_r/S 0.041
Rudder chord, feet 1.76
Aspect ratio of plan form 1
Taper ratio 0
Airfoil section parallel to model
    center line . . . . NACA 0005 (modified)

NACA

TABLE I.- CONCLUDED

```
┌─────────────────────────────────────────────────────────────────────────┐
│ Horizontal tail[1]                                                        │
│                                                                           │
│   $S_t/S$ . . . . . . . . . . . . . . . . . . . . . . . . . . .   0.246   │
│   $b_t/b$ . . . . . . . . . . . . . . . . . . . . . . . . . . .   0.521   │
│   Chord at fuselage center line . . . . . . . . . . . . . . .     5.71    │
│   $l_t/\bar{c}$ . . . . . . . . . . . . . . . . . . . . . . . .   1.735   │
│   Aspect ratio . . . . . . . . . . . . . . . . . . . . . . . .    4.4     │
│   Taper ratio . . . . . . . . . . . . . . . . . . . . . . . .     0.46    │
│   Airfoil section parallel to                                             │
│     model center line  . . . .   modified diamond section (4.2-percent-   │
│                                  chord maximum thickness)                 │
│   Percent chord line having zero                                          │
│     sweep angle  . . . . . . . . . . . . . . . . . . . . . . .    50.0     │
└─────────────────────────────────────────────────────────────────────────┘
```

[1]Pivot line passes through the 27-percent point of the horizontal-
   tail chord in the plane of symmetry.

TABLE II.- SUMMARY OF CONFIGURATIONS TESTED
[W, wing; F, fuselage; V, vertical tail; H, horizontal tail]

Fig-ure	Config-uration	Control deflection (deg) Outboard flaps		Inboard flaps		Horizontal tail		Rudder	β	α	Data
		δ_o	δ_{l_o}	δ_i	δ_{l_i}	i_t	δ_{l_t}	δ_r			
5	W+F+V	0	0	0 / 40	0			0	0,6	-2→25	C_L vs α, C_D, C_m C_L vs C_l, C_n, C_Y
6	W+F+V	0 / 0 / 0 / 0	10 / 20 / 10 / 20	0 / 40	0 / 0			0	0	-2→25	C_L vs α, C_D, C_m C_L vs C_l, C_n, C_Y
7	W+F+V	0	0	0 / 40	0 / 0			0	-2→12	0,6,12, 18,24	C_L, C_D vs β C_l, C_m vs β C_Y, C_n vs β
8	W+F+V	0	0	5 / 35	10 / 10			0	0	-2→25	C_L vs α, C_D, C_m C_L vs C_l, C_n, C_Y
	W+F+V+H	0	0	5 / 35	10 / 10	-10	0				
9	W+F+V	0	0	0 / 30	20 / 20			0	0	-2→25	C_L vs α, C_D, C_m C_L vs C_l, C_n, C_Y
	W+F+V+H	0	0	0 / 30	20 / 20	-10	0				
10	W+F+V+H	0	0	0	0	0 / -10 / -10	0 / 0 / 20	0	0	-2→25	C_L vs α, C_D, C_m C_L vs C_l, C_n, C_Y
				40	0	0 / -10 / -10	0 / 0 / 20				
11	W+F+V+H	0	0	40	0	-10 / -10 / -10	0 / 10 / 20	10	0	-2→25	C_L vs α, C_D, C_m C_L vs C_l, C_n, C_Y
12	W+F+V+H	0	0	0 / 40	0 / 0	-10	0	0	-2→12	0,6,12 18,24	C_L, C_D vs β C_l, C_m vs β C_Y, C_n vs β
13	W+F+V	0 / 20 / 30 / 40	0 / 0 / 0 / 0	40	0			0	0	-2→25	C_L vs α, C_D, C_m

Note: All force and moment coefficients, angles and control-surface deflections are shown as positive.
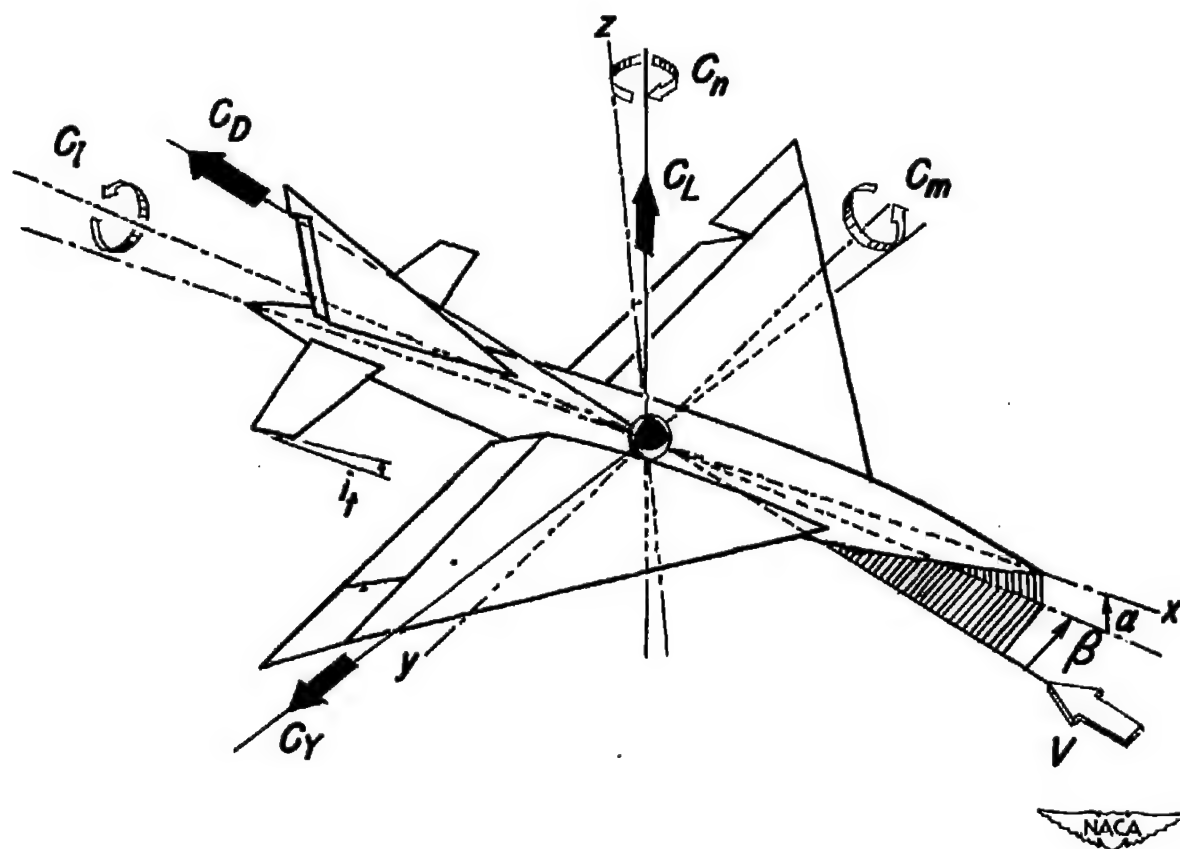
Figure 1.— Sign convention for force and moment coefficients.

9.46°

17.68

9.22

$\bar{c} = 11.78$

45°

11.78

$\frac{\bar{c}}{4}$

8.84

5.90

17.68

23.91

22.30 — Pivot line

26.24

17.92

63.43°

8.96

56.16

Dimensions shown in feet
unless otherwise specified

NACA
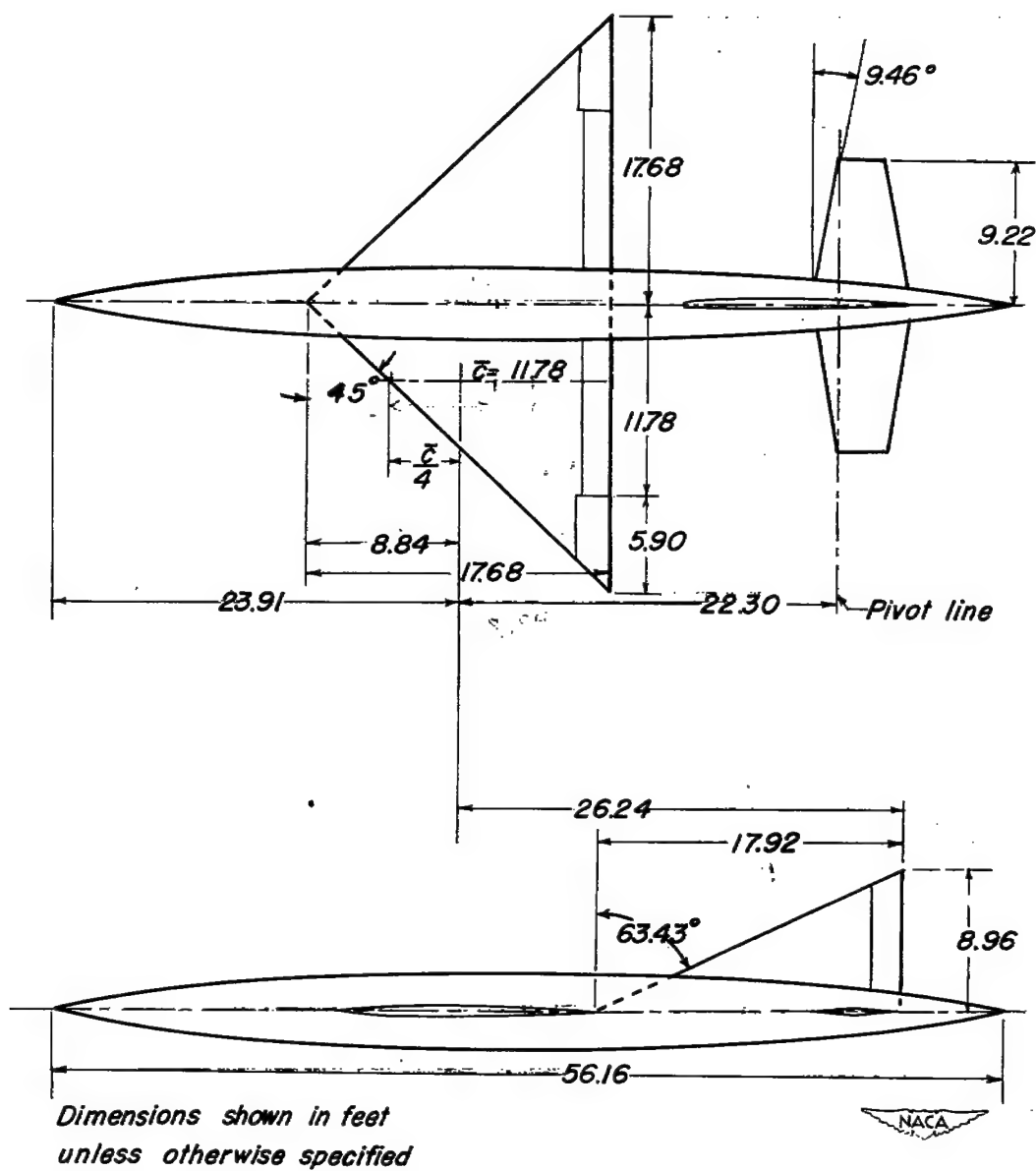
Figure 2.— Geometric details of the model.
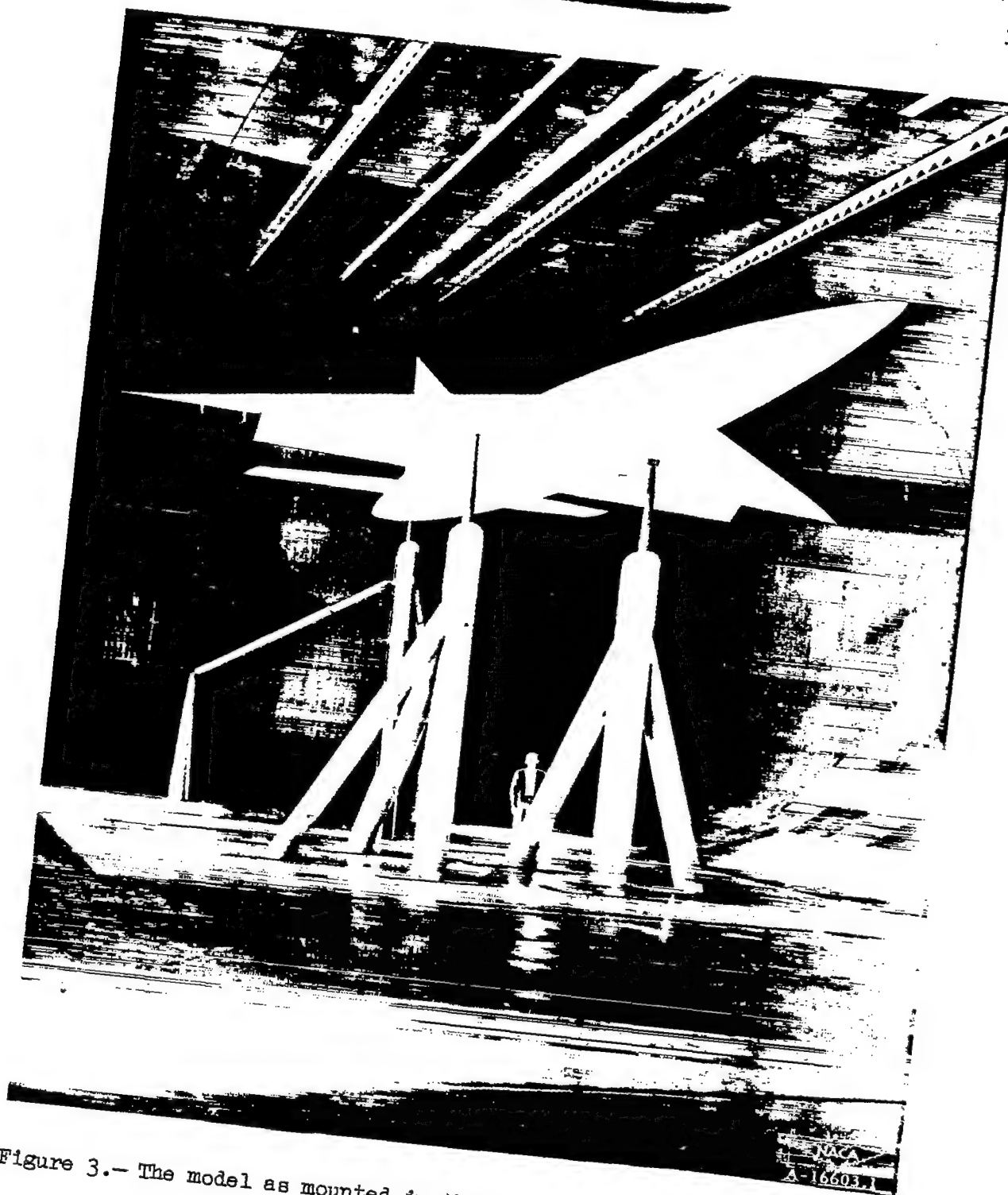
Figure 3.— The model as mounted in the Ames 40— by 80-foot wind tunnel.
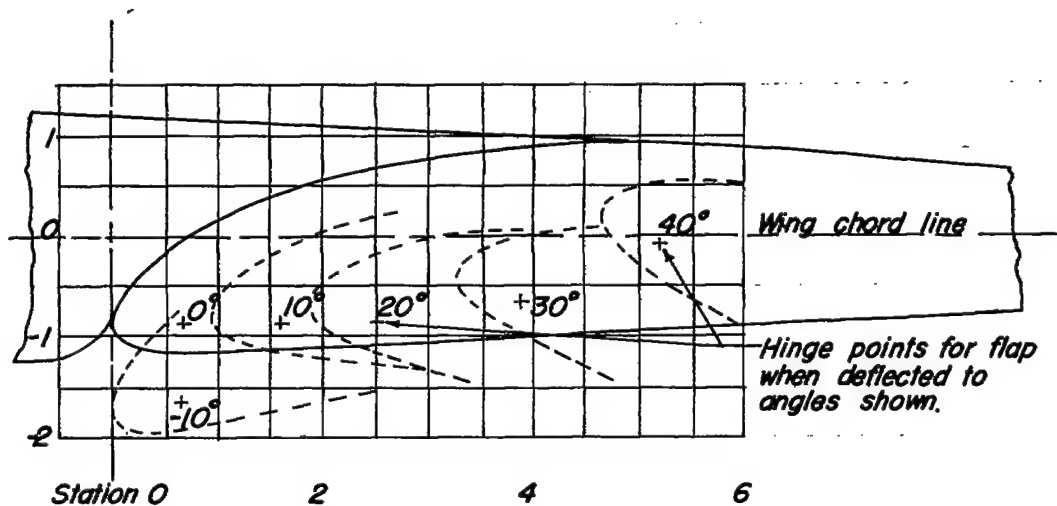
Flap coordinates		
Station	Upper surface	Lower surface
0	−0.872	−0.872
0.113	−.554	−1.030
.226	−.408	−1.086
.452	−.181	−1.119
.679	−.012	−1.131
1.357	.351	−1.119
2.036	.589	−1.086
2.714	.747	−1.041
3.393	.860	−1.006
4.071	.905	−0.973
4.750	.916	−0.938
5.654	.905	−0.905
11.309	.610	−0.610
16.963	.328	−0.328
23.560	0	0
Center of L.E. arc		
0.17	−0.87	
L.E. radius: 0.17		

Dimensions shown in inches.

Figure 4.— Details of the slotted inboard flaps.
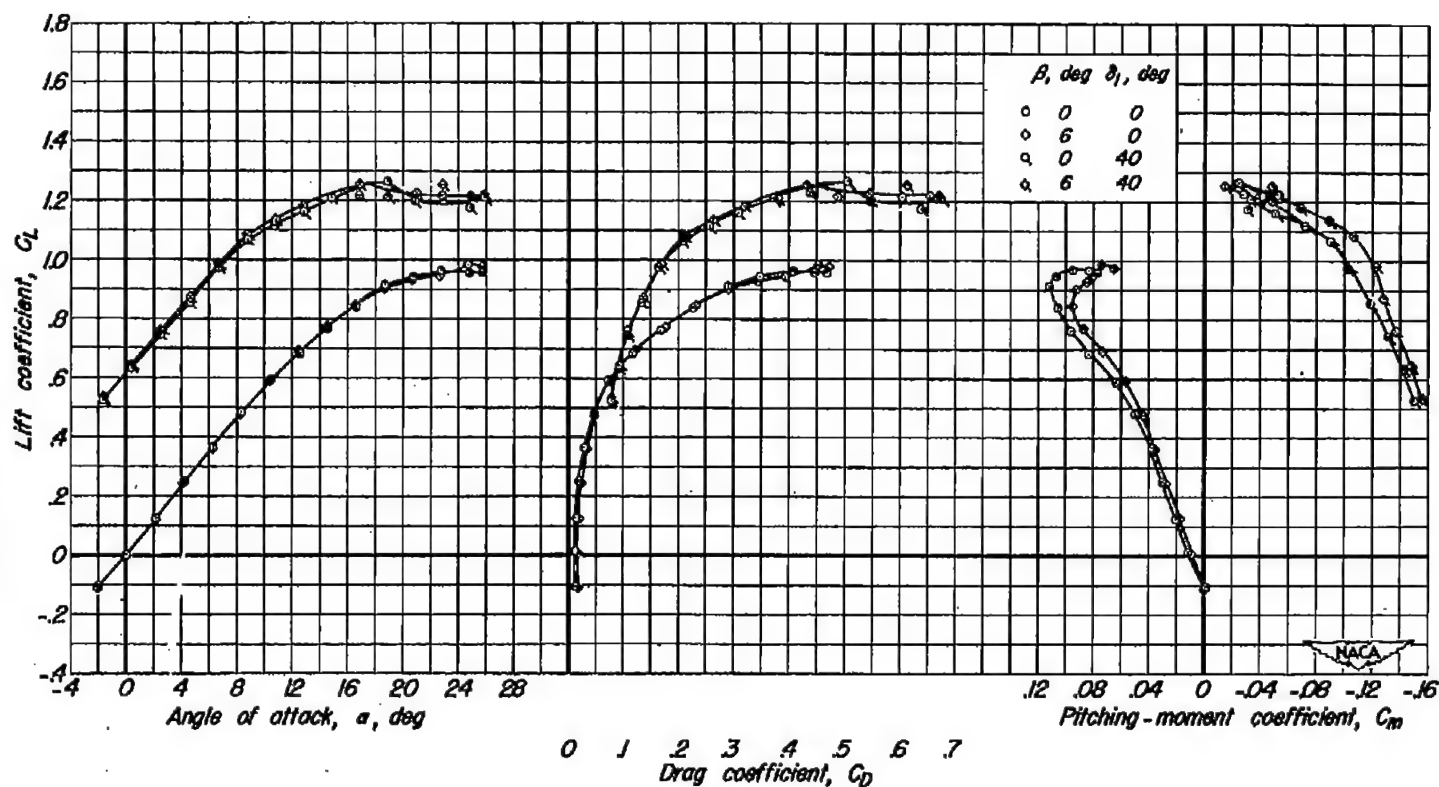
(a) C_L vs a, C_D, C_m

Figure 5.— Characteristics of the wing-fuselage – vertical-tail configuration at two angles of sideslip and with two inboard flap deflections.

	β, deg	δ_l, deg
○	0	0
◇	6	0
⊘	0	40
⬦	6	40
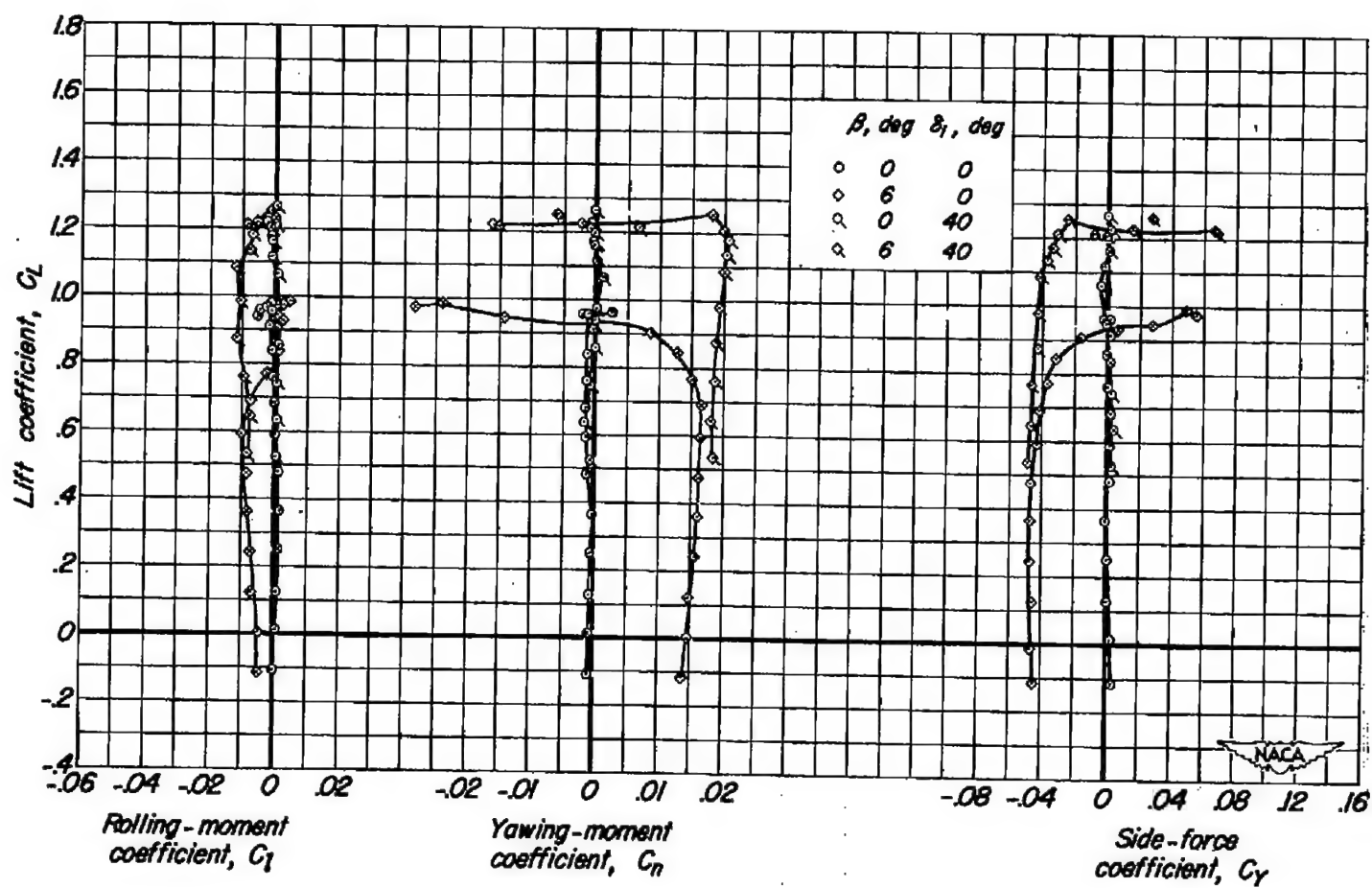
(b) C_L vs C_l, C_n, C_Y

Figure 5.- Concluded.

(a) C_L vs a, C_D, C_m
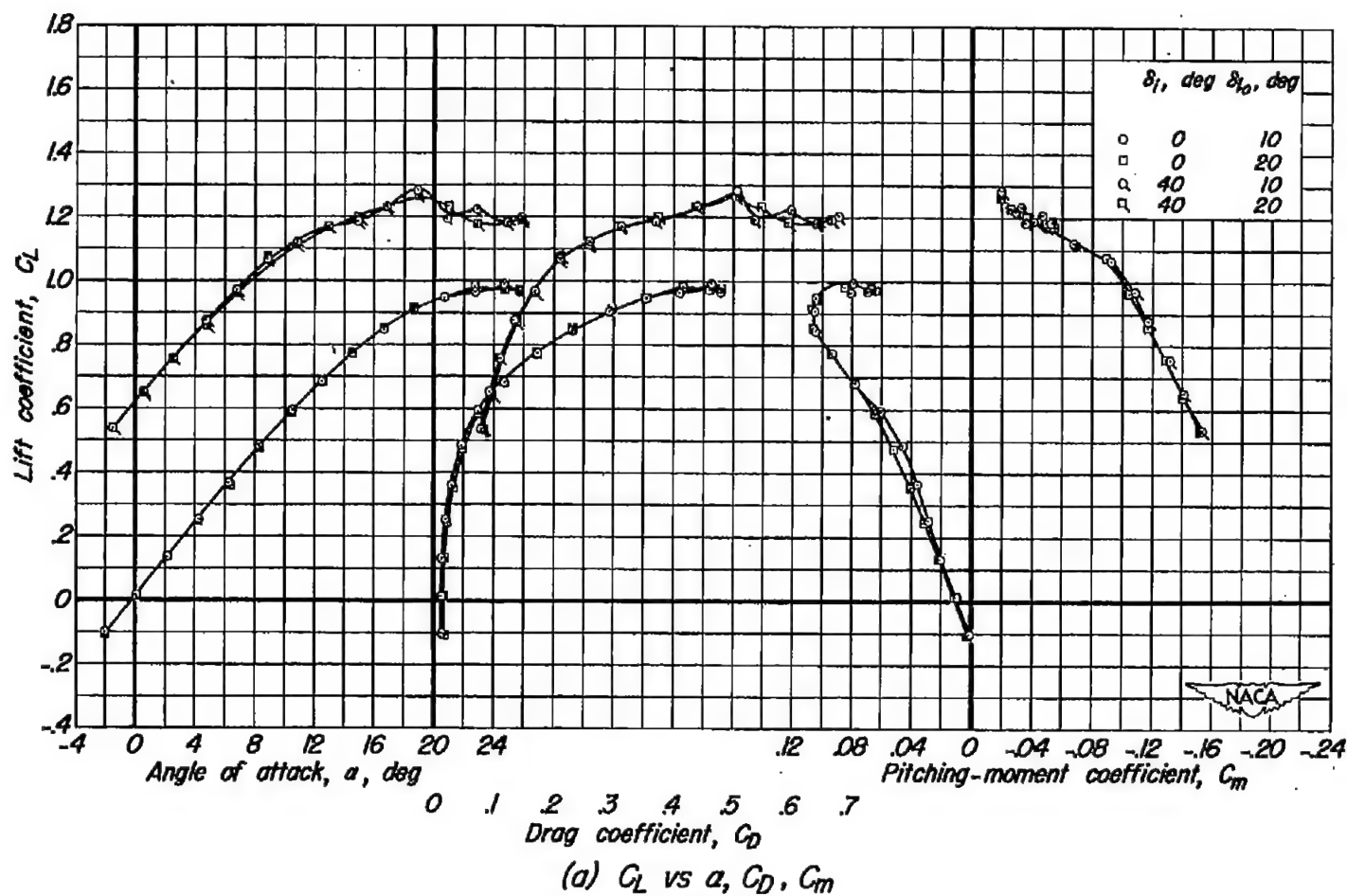
Figure 6.— Characteristics of the wing-fuselage – vertical-tail configuration with the outboard flaps differentially deflected. δ_o, $0°$.

δ_i, deg	δ_{i_o}, deg
0	10
0	20
40	10
40	20
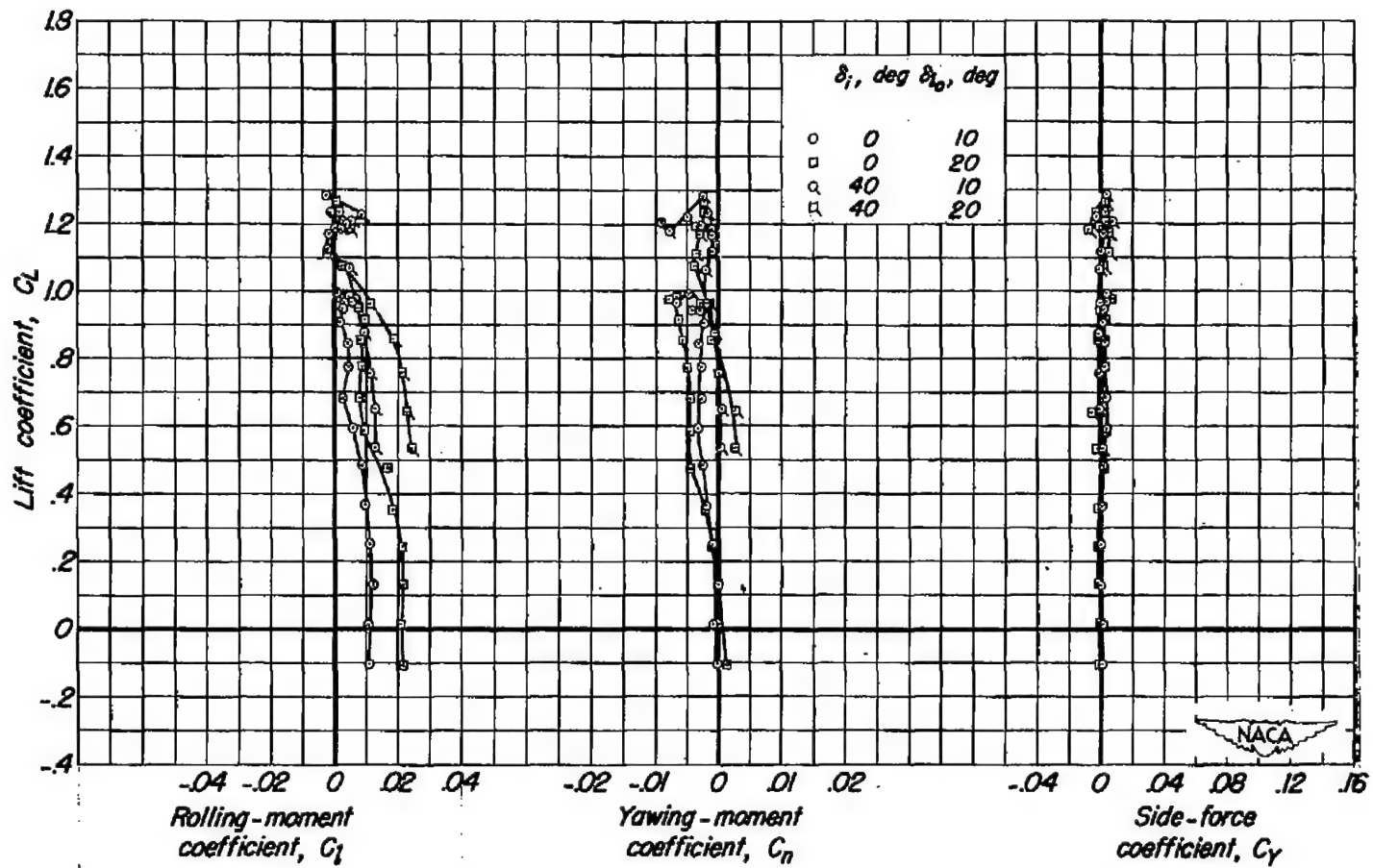
(b) C_L vs C_l, C_n, C_Y

Figure 6.- Concluded.
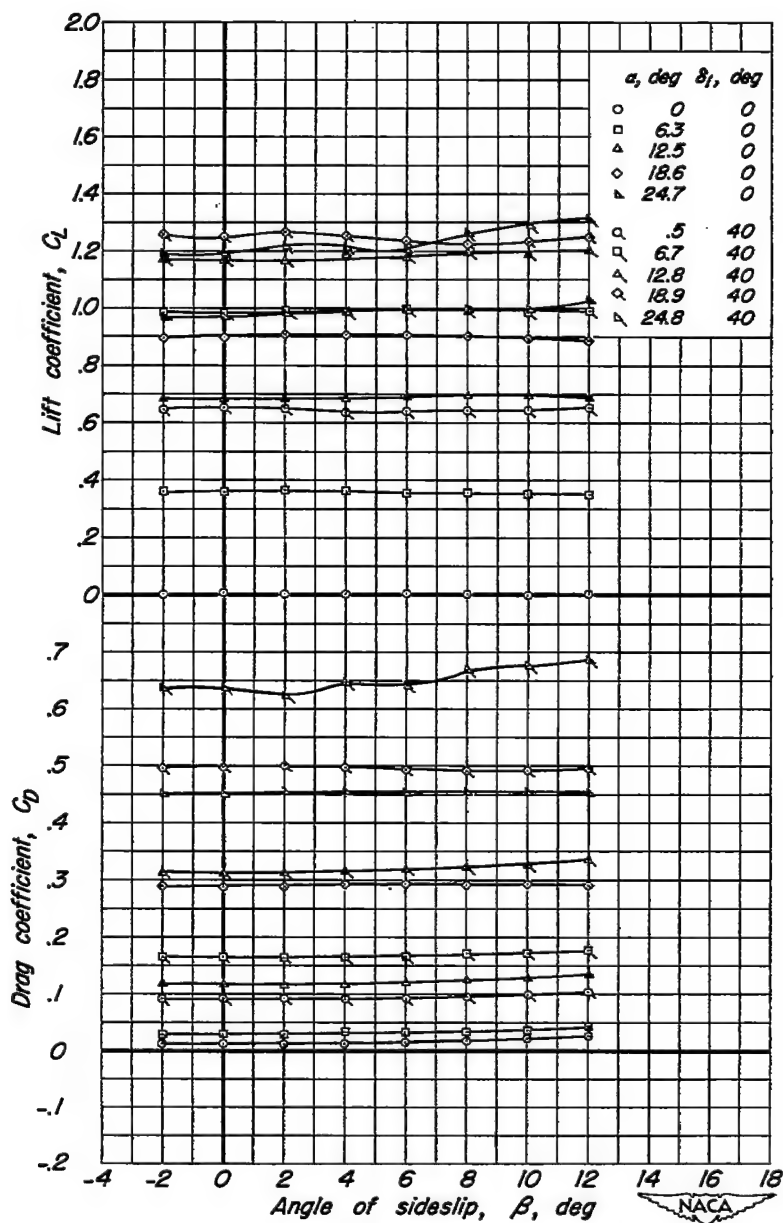
(a) C_L, C_D vs β

Figure 7.— Characteristics in sideslip of the wing-fuselage — vertical-tail configuration with two inboard-flap deflections.
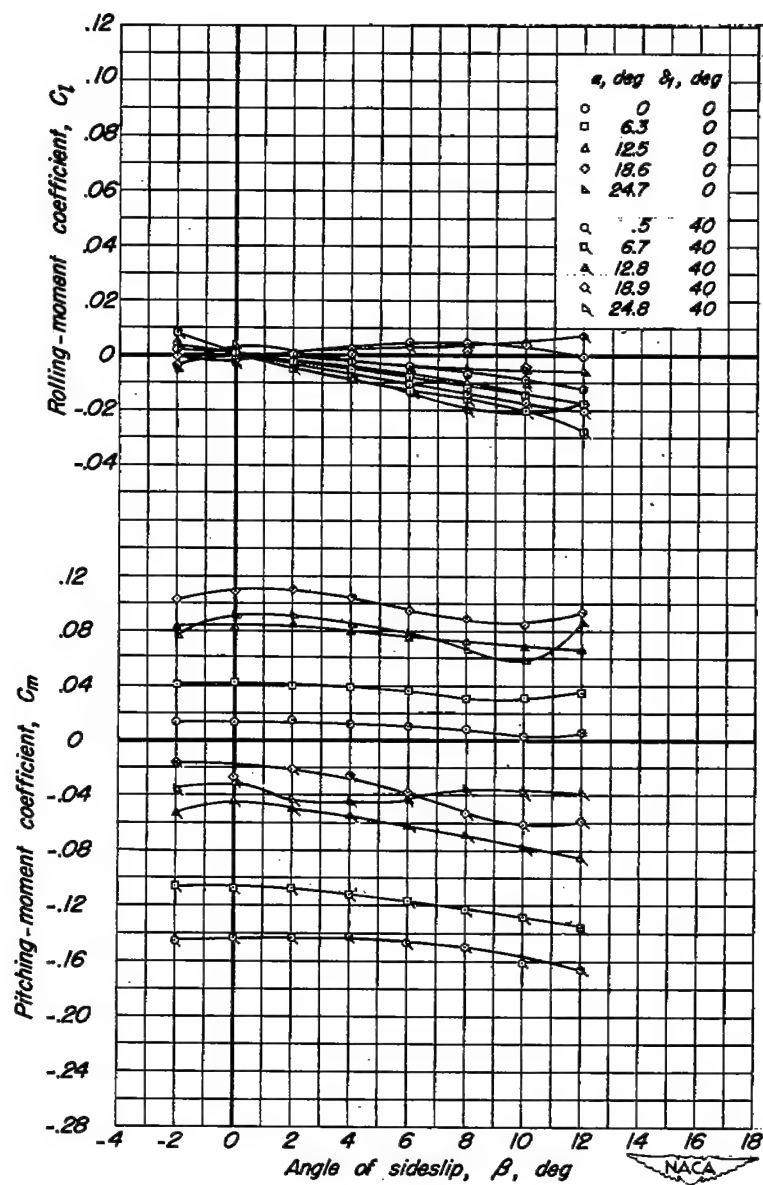
(b) C_l, C_m vs β

Figure 7.— Continued.
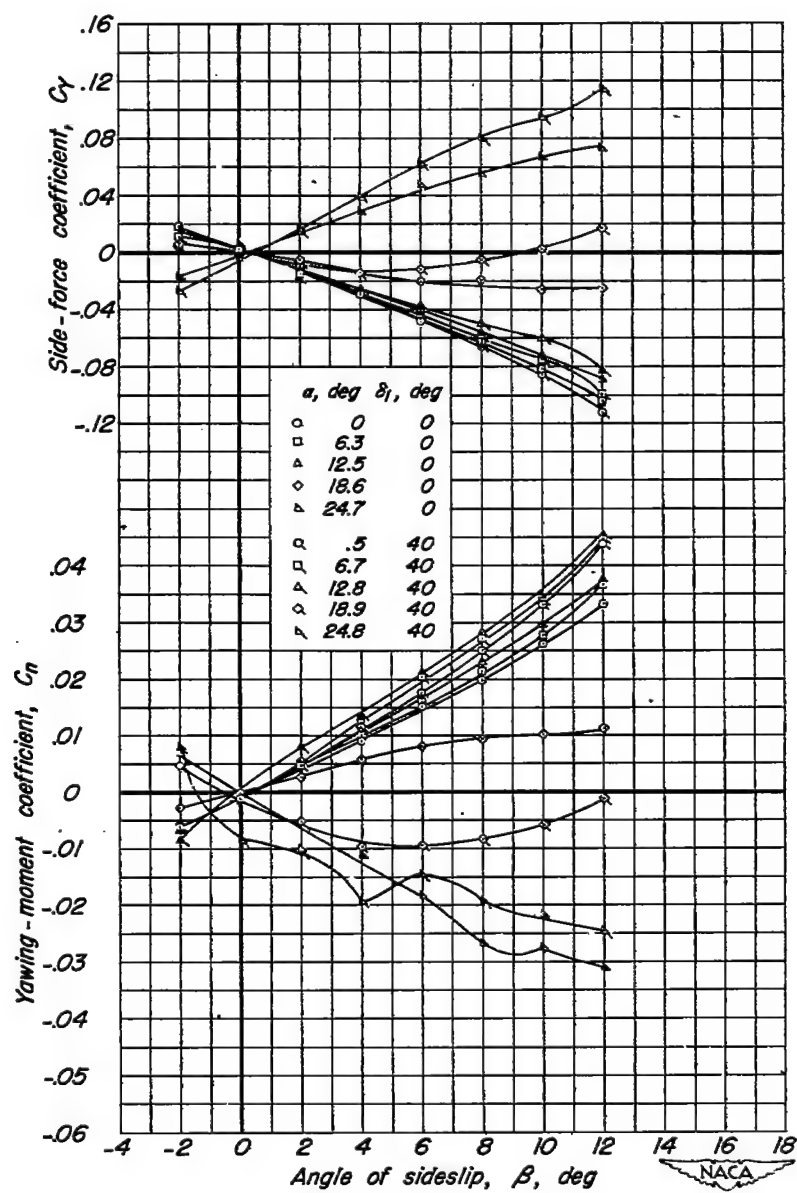
(c) C_Y, C_n vs β

Figure 7.— Concluded.
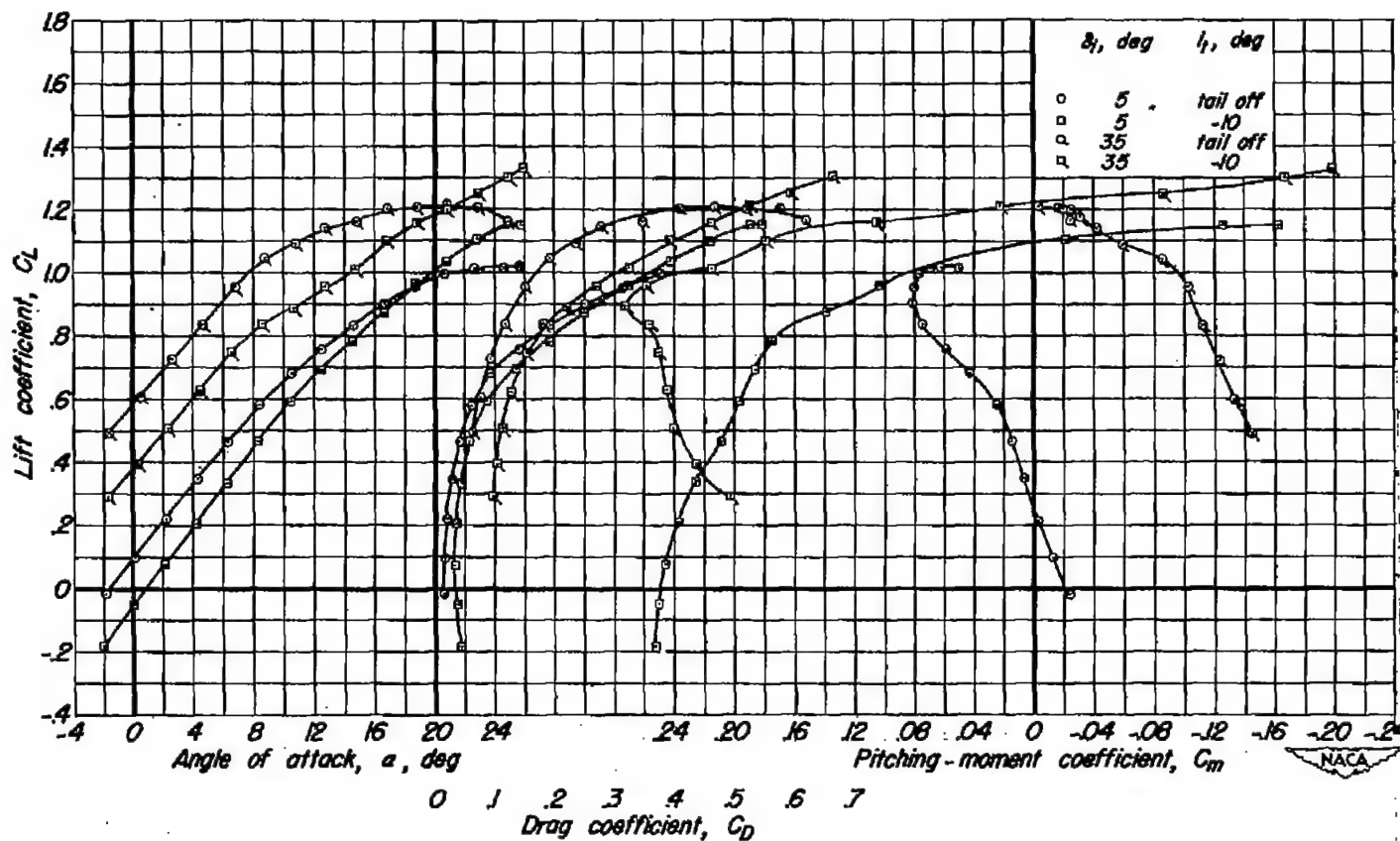
(a) C_L vs a, C_D, C_m

Figure 8.— Characteristics of the wing—fuselage—vertical—tail configuration and the complete airplane model with the inboard flaps differentially deflected. δ_{i_j}, $10°$

δ_l, deg	i_t, deg
5	tail off
5	-10
35	tail off
35	-10
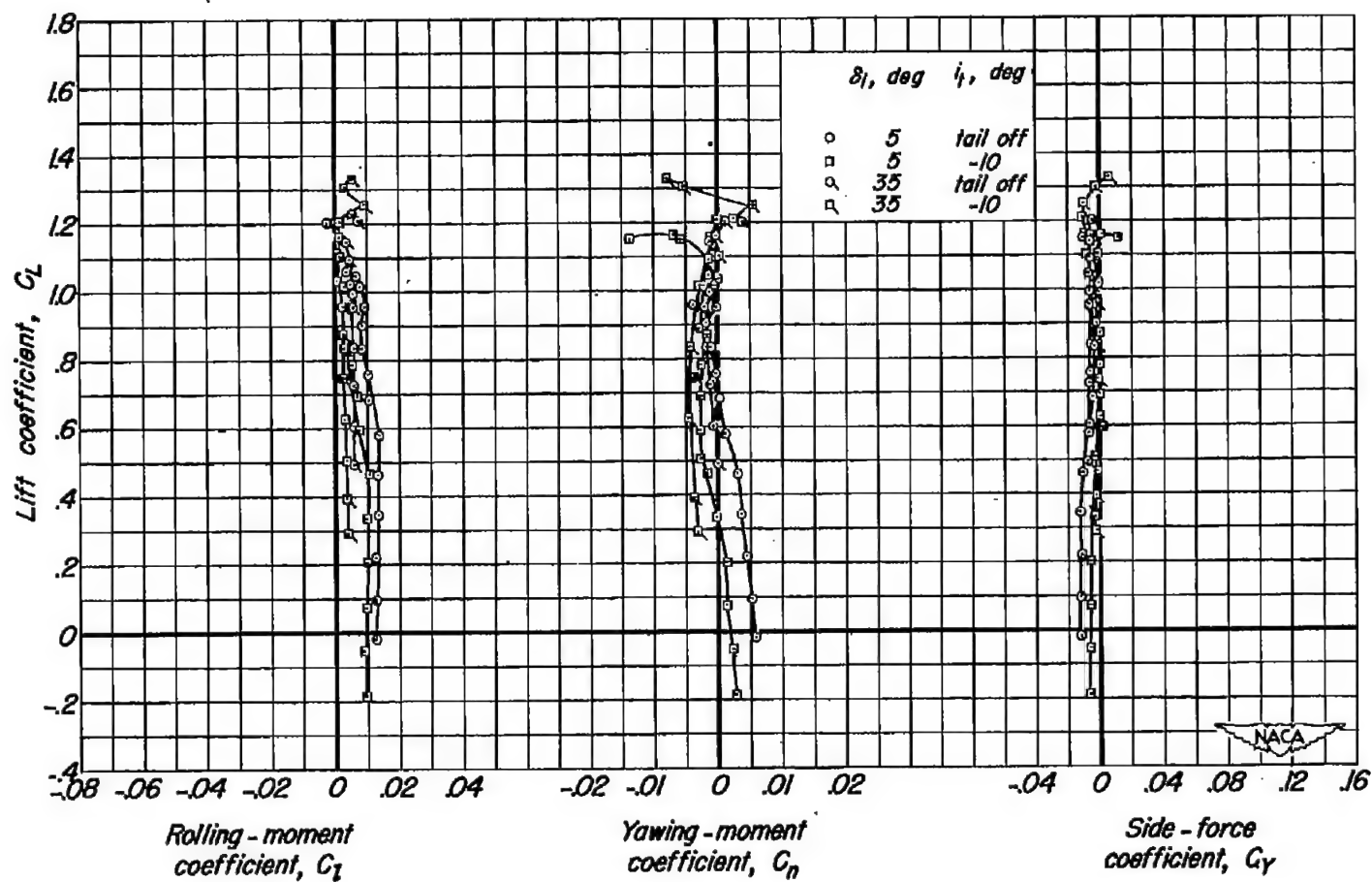
(b) C_L vs C_l, C_n, C_Y

Figure 8.— Concluded.
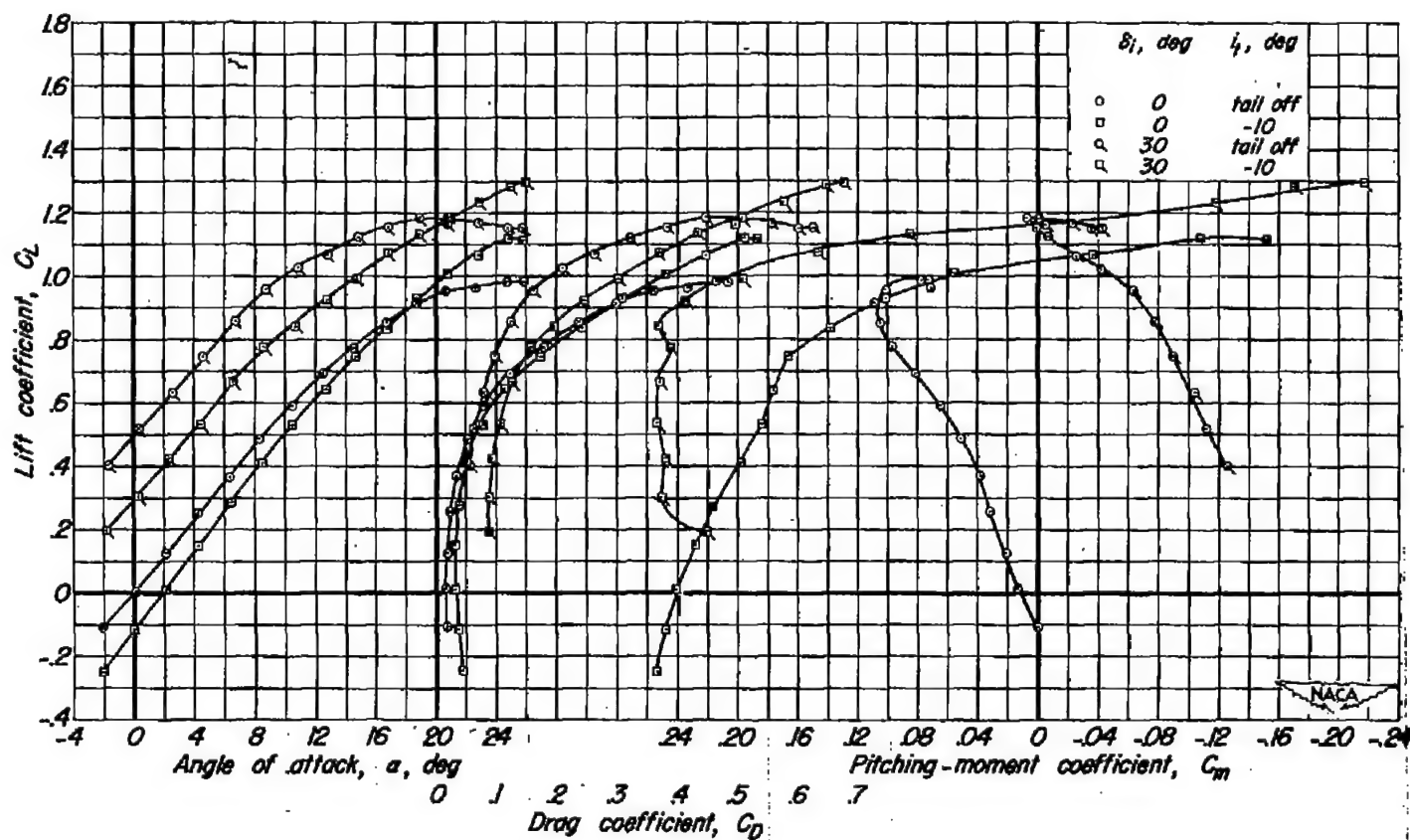
(a) C_L vs a, C_D, C_m

Figure 9.— Characteristics of the wing—fuselage—vertical—tail configuration and the complete airplane model with the inboard flaps differentially deflected. δ_{i_j}, 20.°
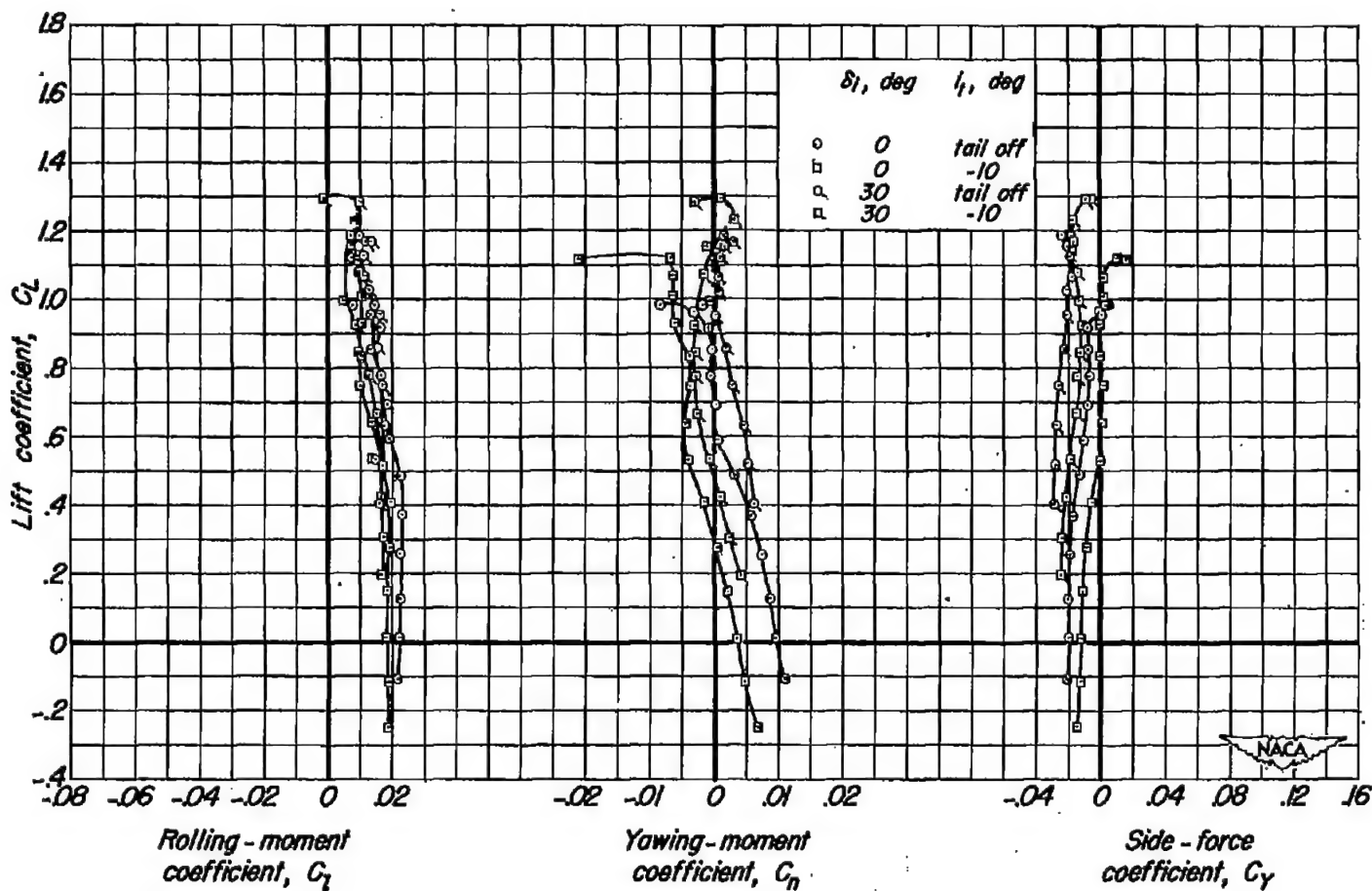
(b) C_L vs C_l, C_n, C_Y

Figure 9.— Concluded.
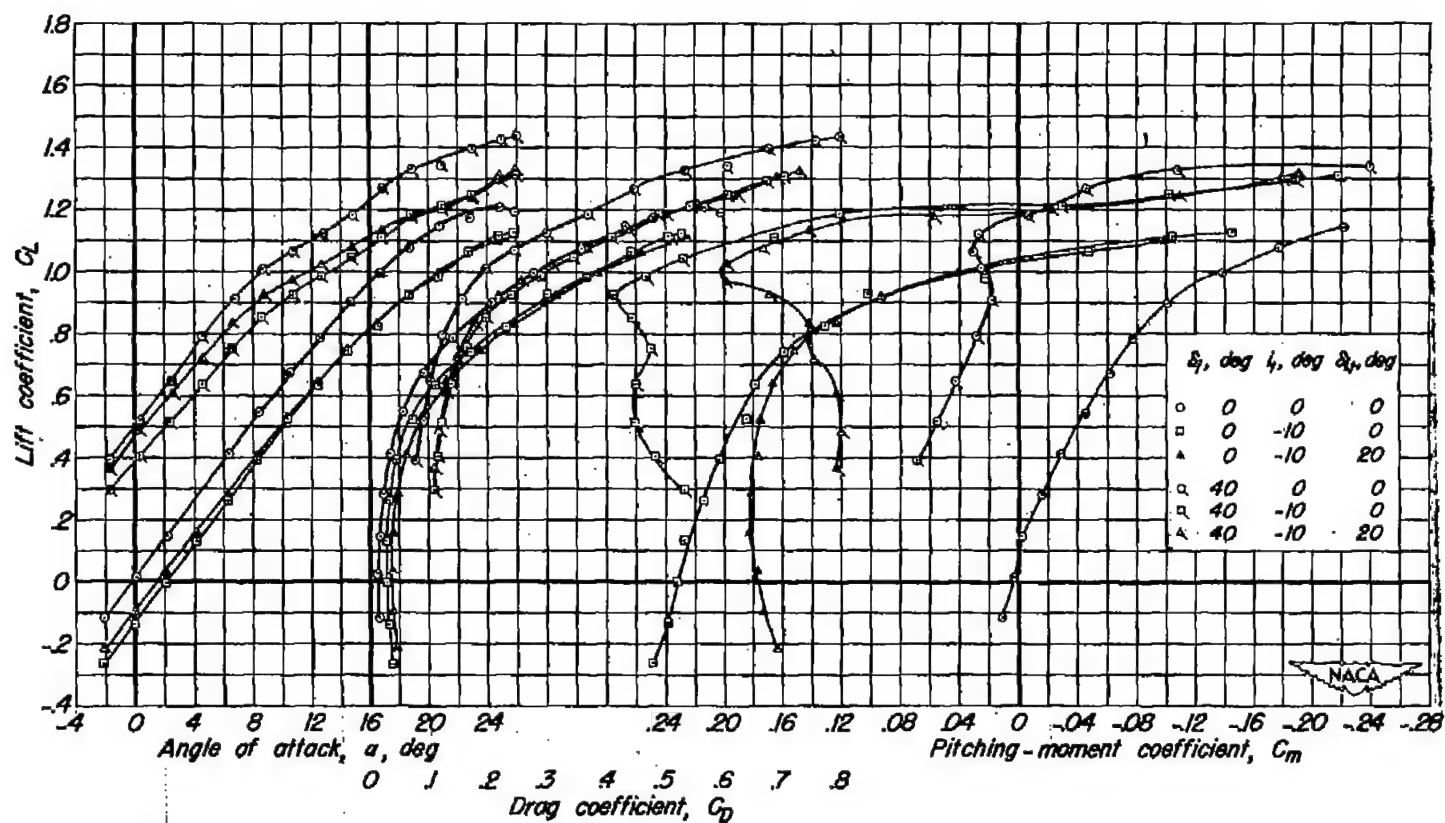
(a) C_L vs α, C_D, C_m

Figure 10.— Characteristics of the model with the horizontal tail differentially deflected.

δ_l, deg	i_t, deg	δ_{tf}, deg
0	0	0
0	-10	0
0	-10	20
40	0	0
40	-10	0
40	-10	20
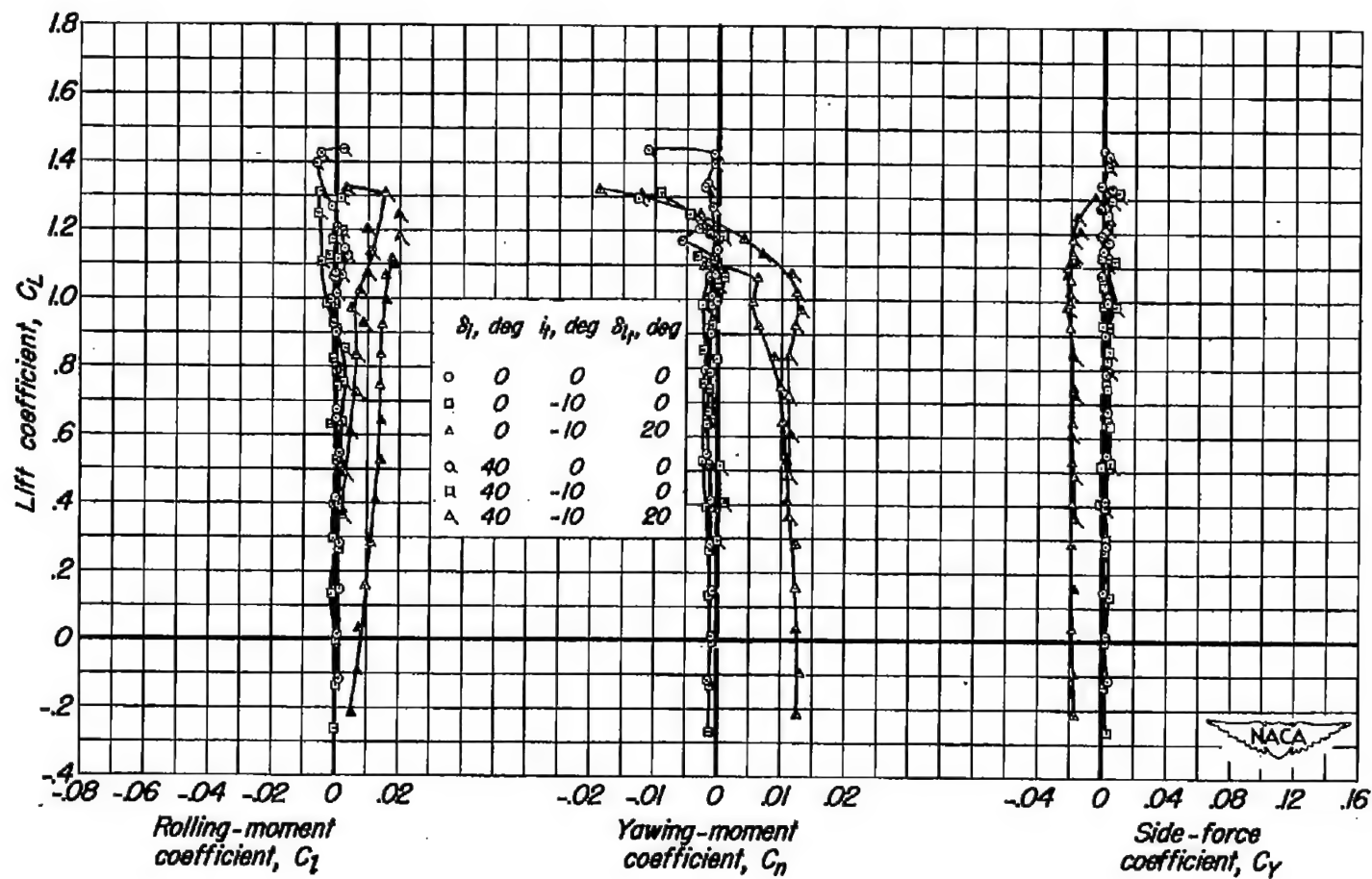
(b) C_L vs C_l, C_n, C_Y

Figure 10.— Concluded.
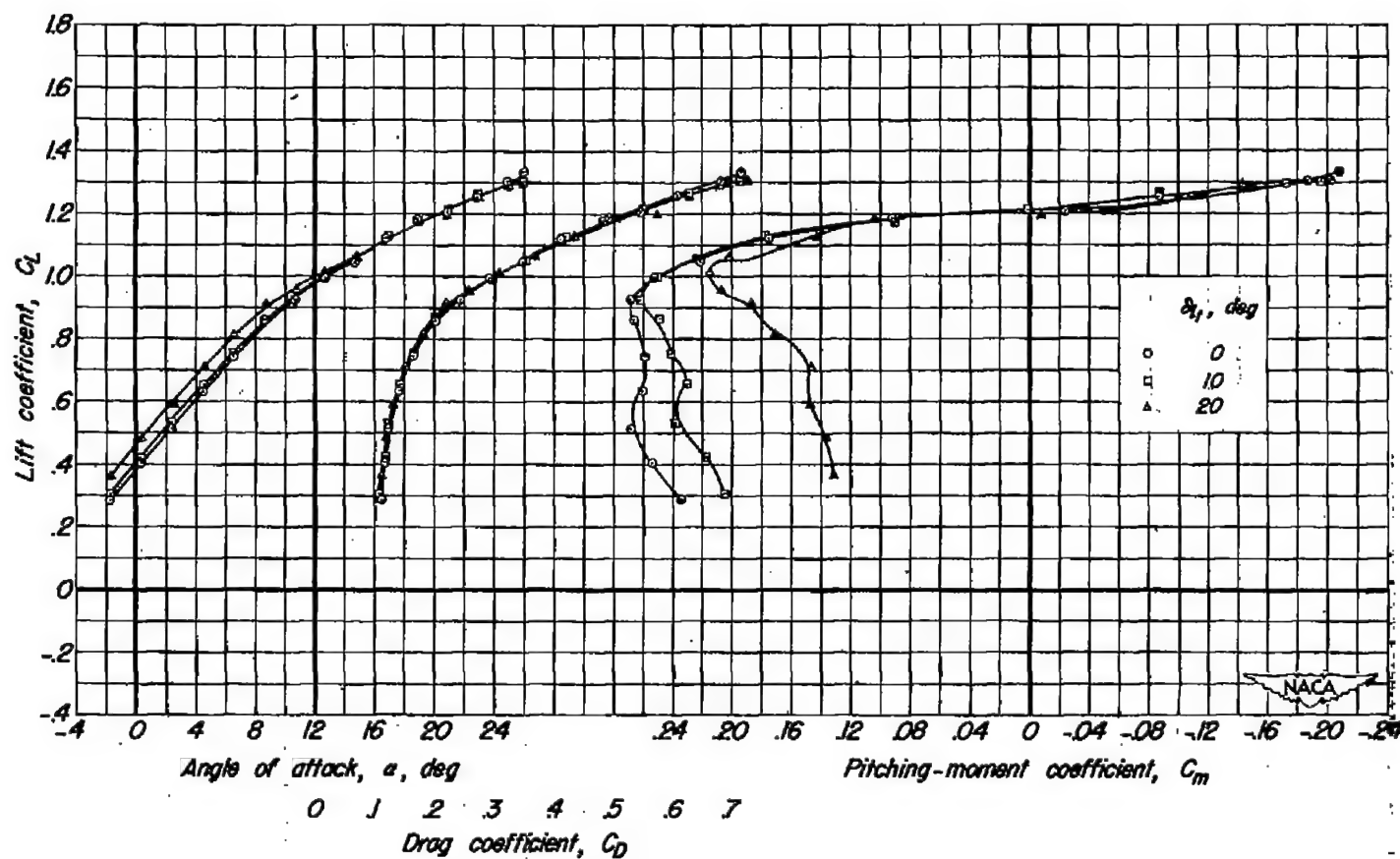
(a) C_L vs α, C_D, C_m

Figure II.— Characteristics of the model with the horizontal tail differentially deflected. δ_r, 10°.
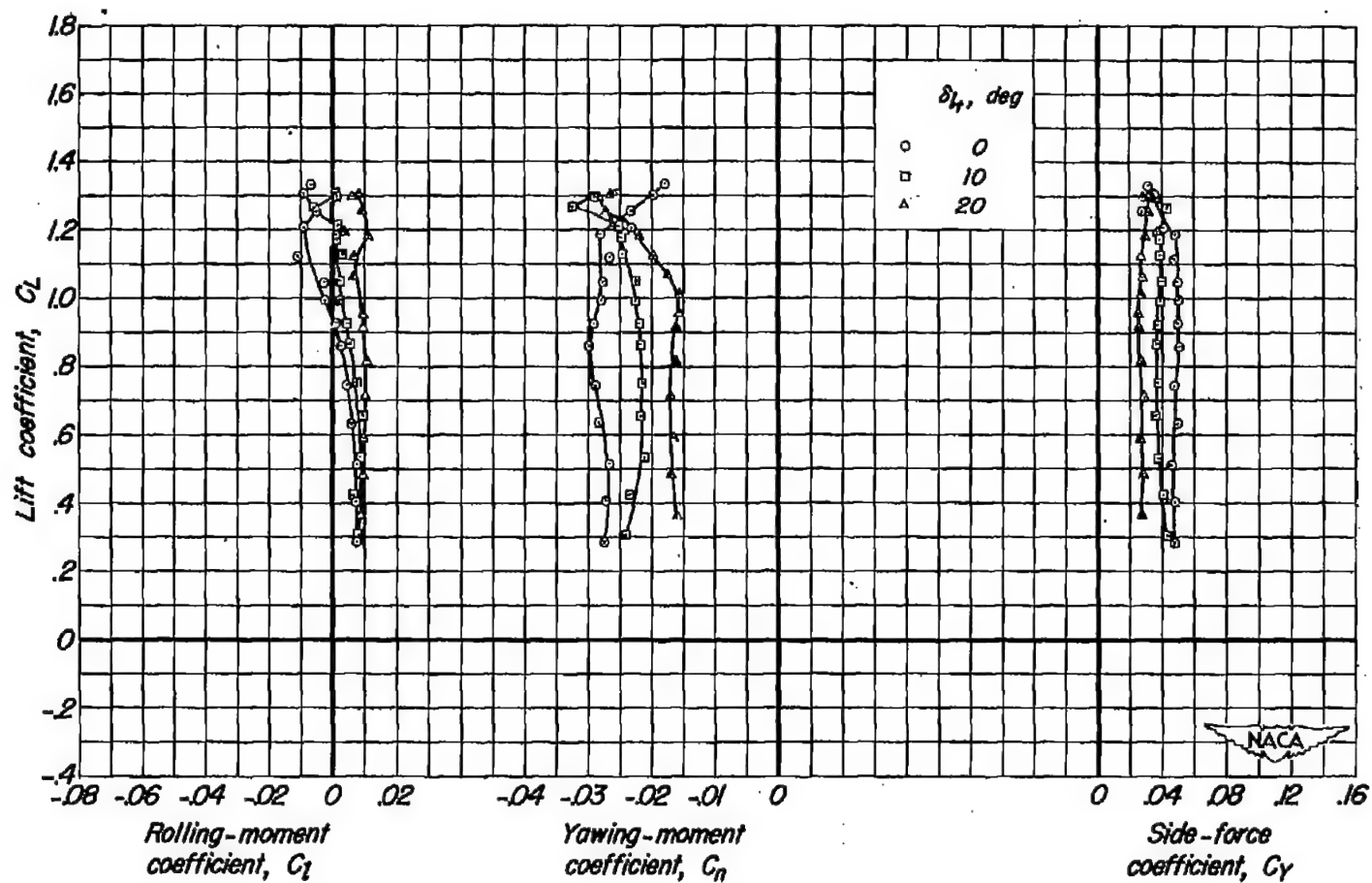
(b) C_L vs C_l, C_n, C_Y

Figure 11.— Concluded.

a, deg	δ_i, deg
0	0
6.2	0
12.5	0
18.7	0
24.8	0
.3	40
6.6	40
12.7	40
18.8	40
24.9	40
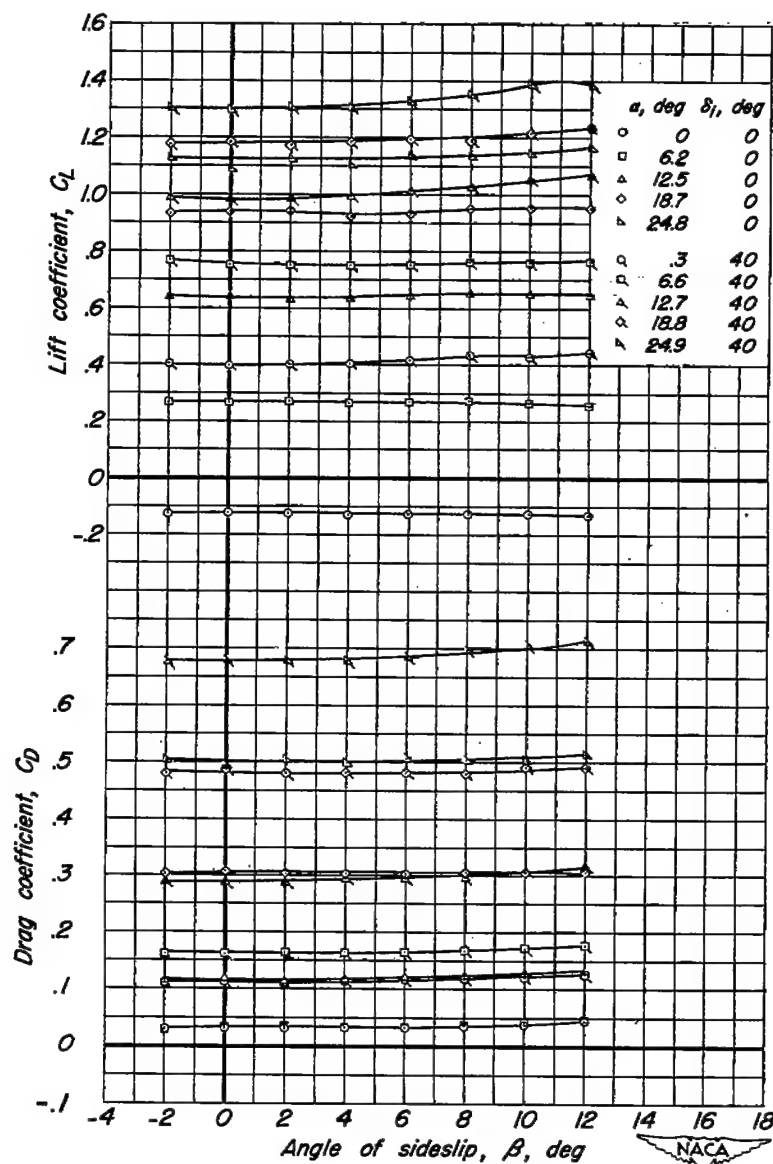
(a) C_L, C_D vs β

Figure 12.— Characteristics in sideslip of the complete model with two inboard-flap deflections. i_f, -10°.

	a, deg	δ_l, deg
○	0	0
□	6.2	0
△	12.5	0
◇	18.7	0
◺	24.8	0
○	.3	40
◻	6.6	40
◿	12.7	40
◈	18.8	40
◹	24.9	40
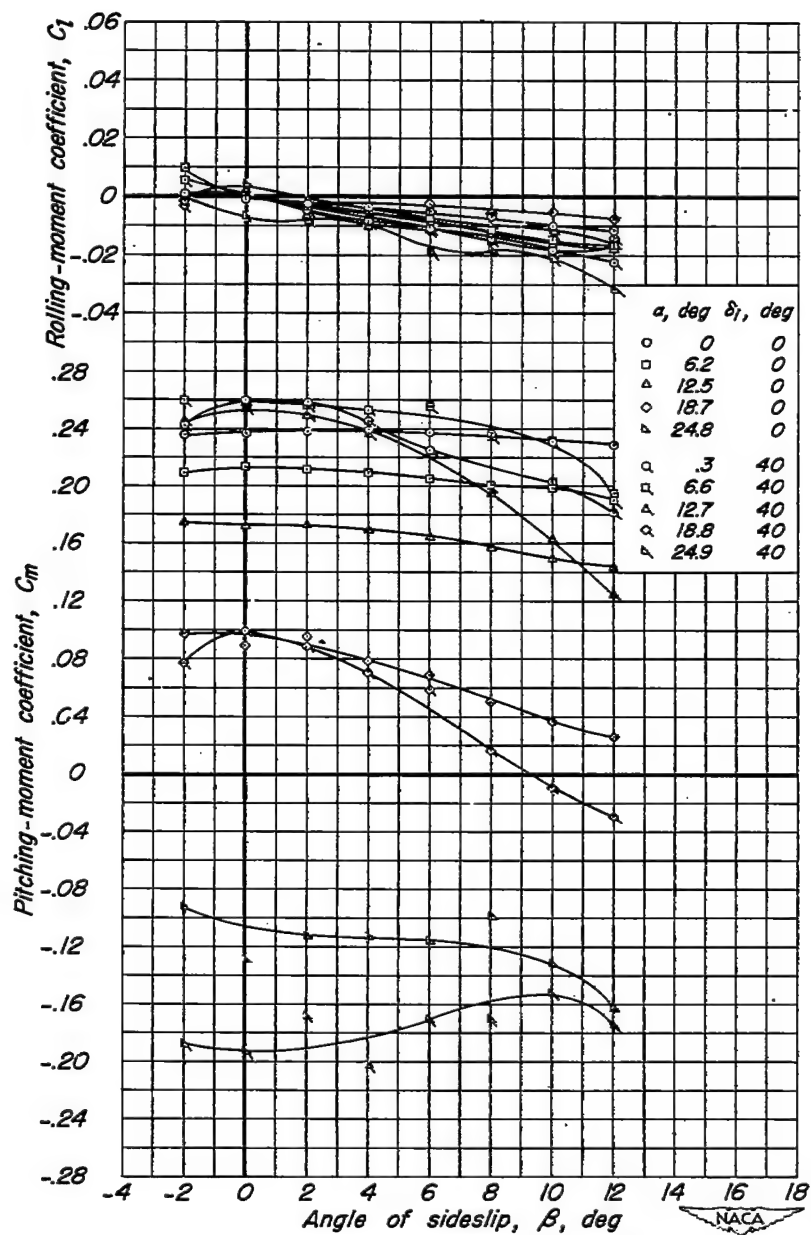
(b) C_l, C_m vs β

Figure 12.- Continued.
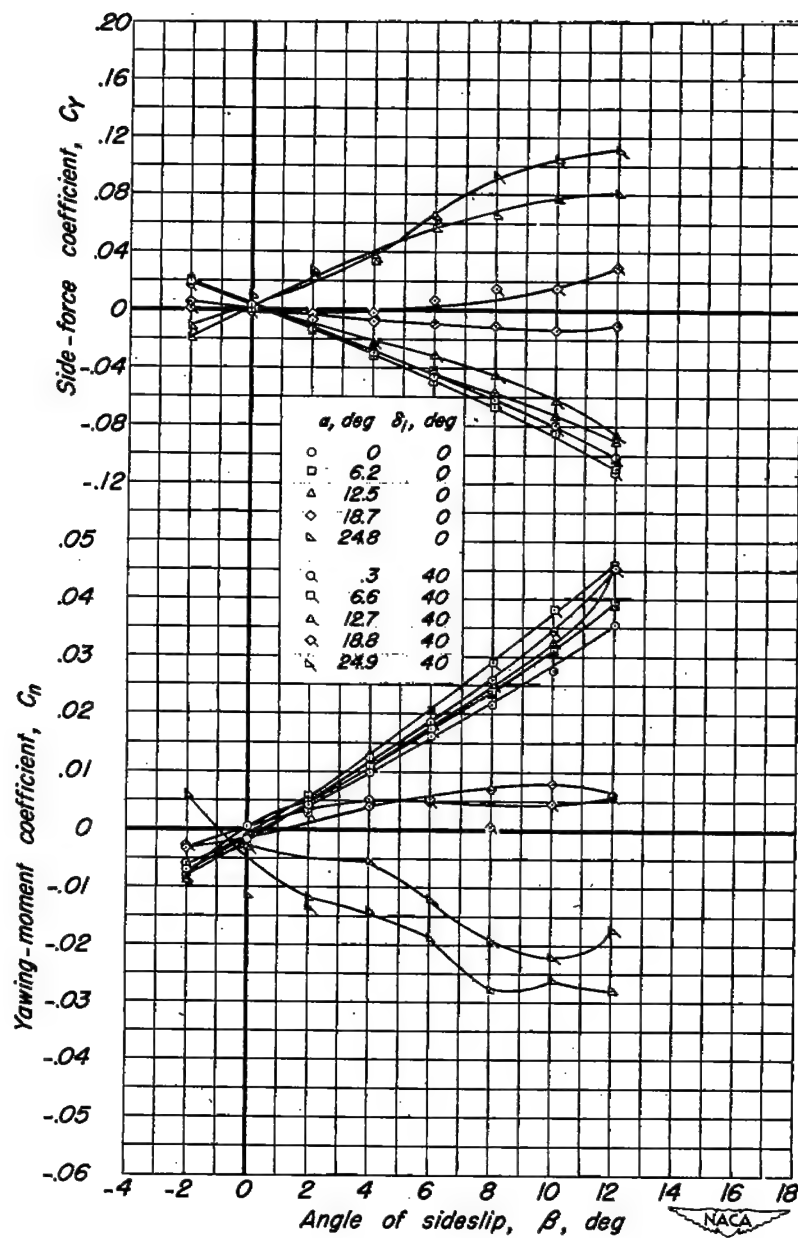
(c) C_Y, C_n vs β

Figure 12.— Concluded.
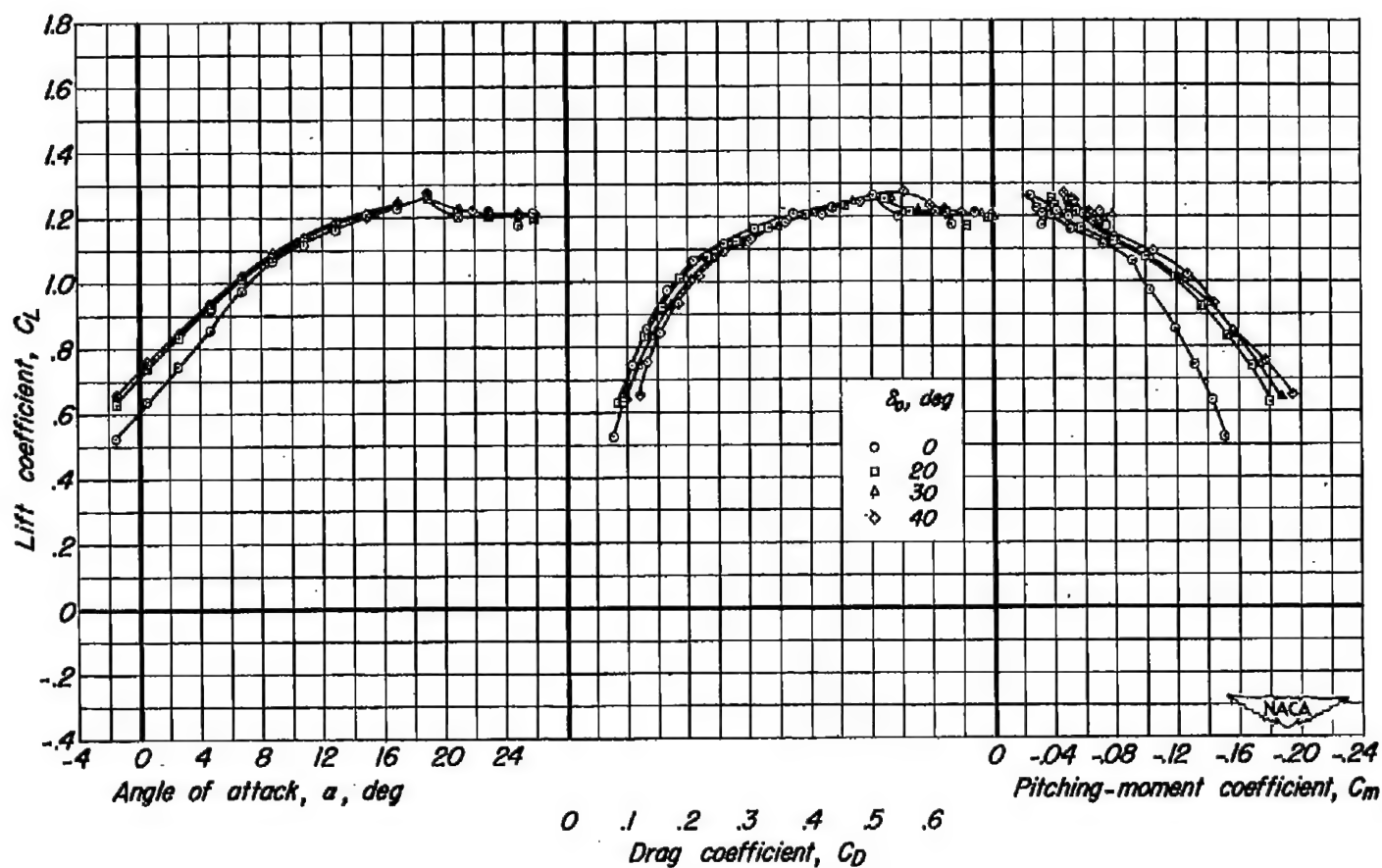
C_L vs a, C_D, C_m

Figure 13.— Characteristics of the wing-fuselage-vertical-tail configuration with the outboard flaps deflected symmetrically. δ_i, 40°.
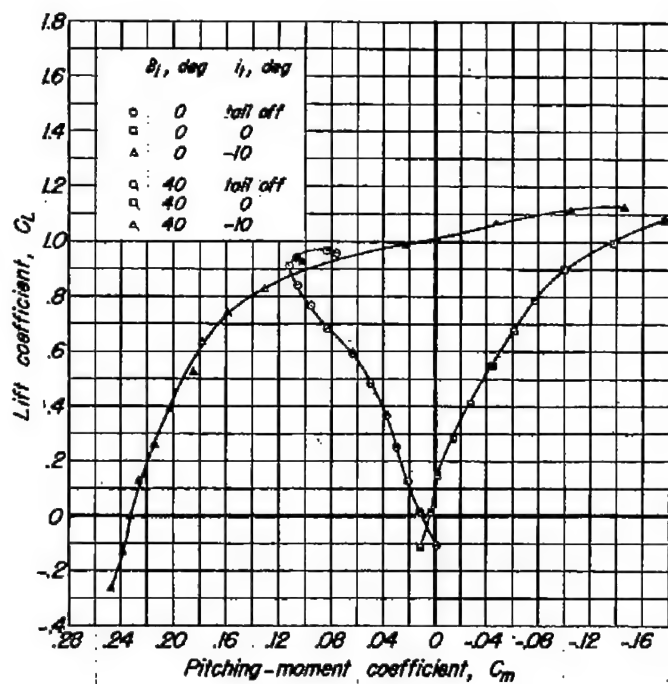
(a) Inboard flaps undeflected.
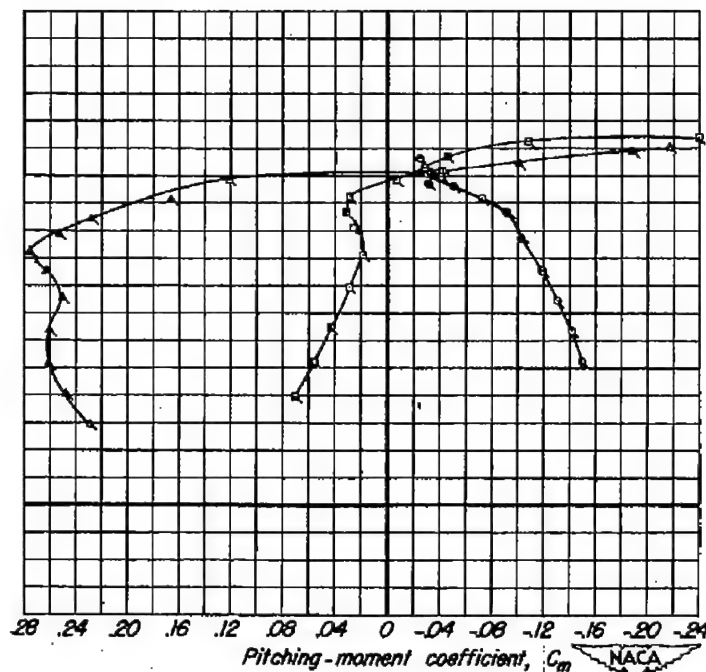
(b) Inboard flaps deflected 40°.

Figure 14.— Longitudinal stability characteristics of the model as affected by the horizontal tail and inboard flaps.
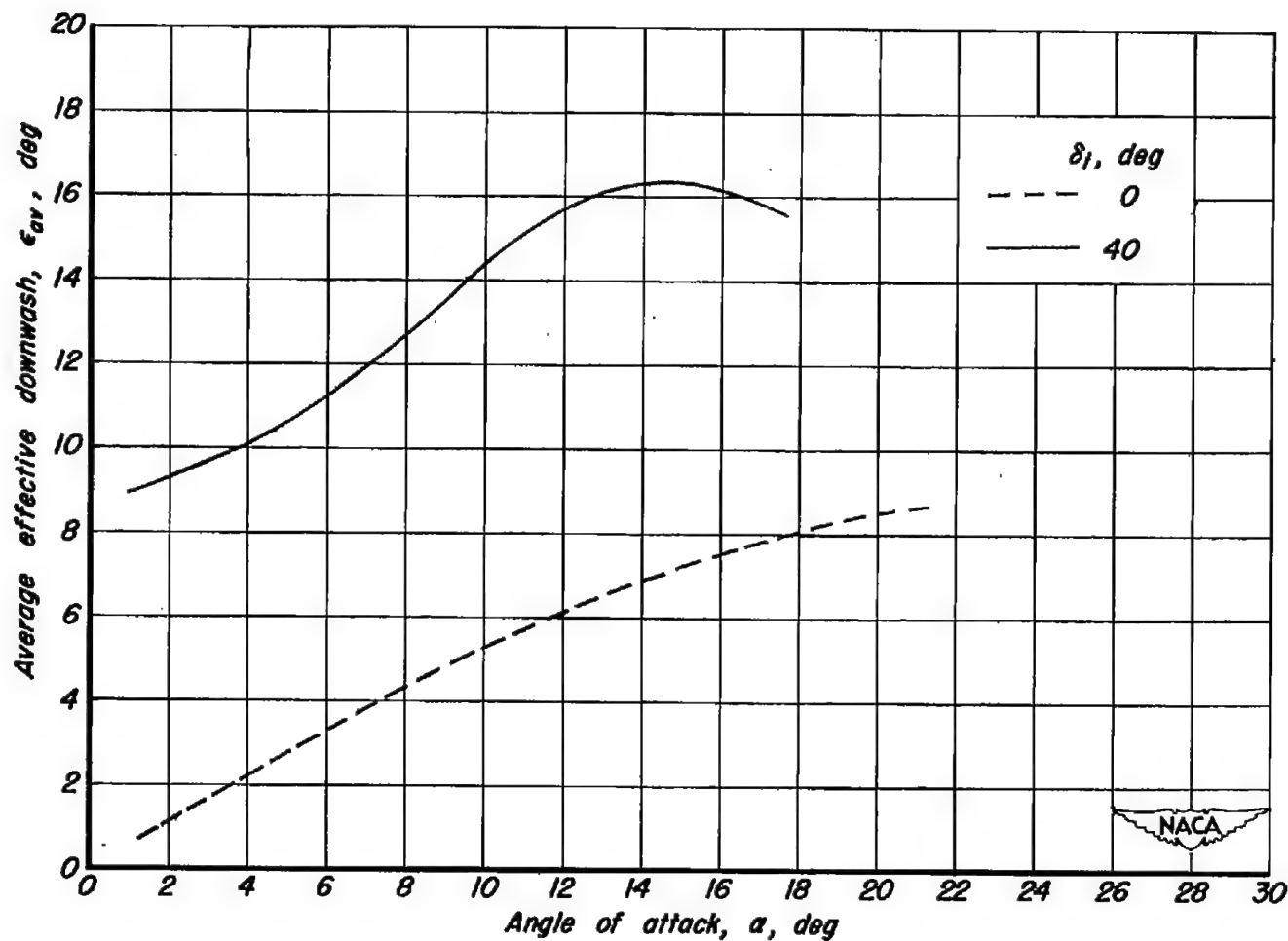
Figure 15.— Variation of average effective downwash angle with angle of attack for two inboard flap deflections.
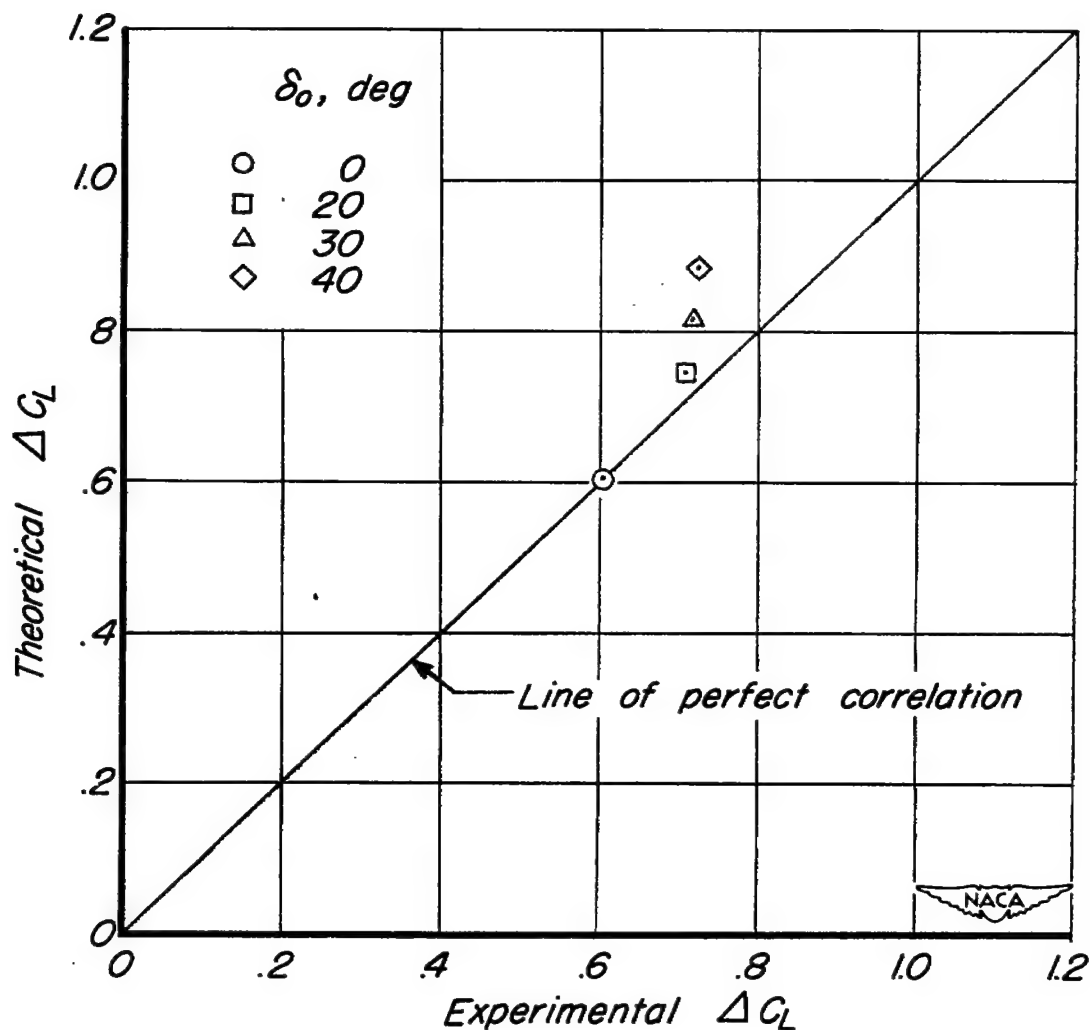
Figure 16.— Experimental and theoretical increments of lift coefficient for deflections of outboard flaps in combination with a deflection of the inboard flaps. a, $0°$; δ_i, $40°$; wing-fuselage-vertical-tail configuration.
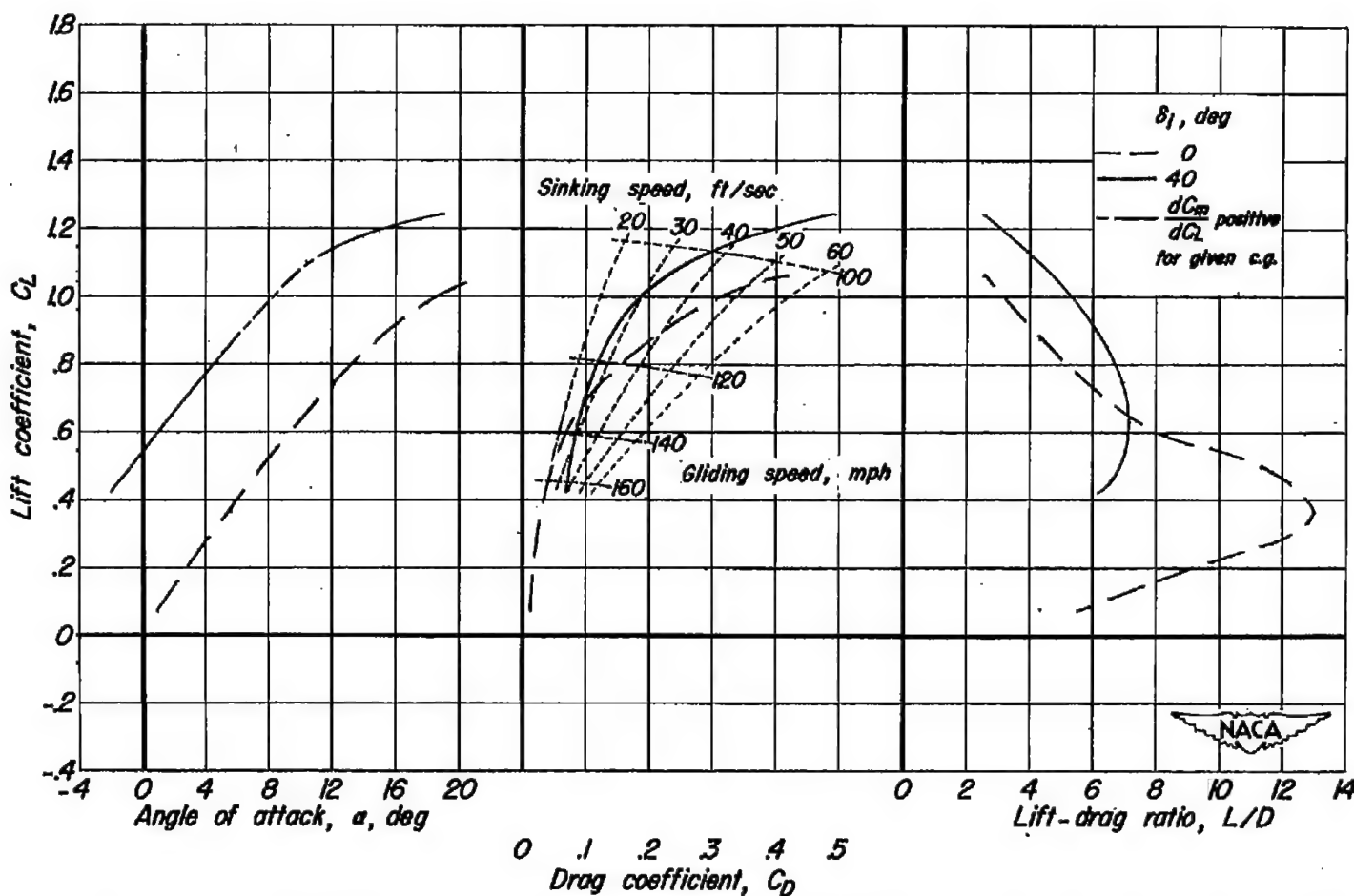
Figure 17.— Comparison of the lift and drag characteristics of the trimmed model without flaps with those of the same model having inboard flaps deflected to 40°. W/S, 30 pounds per square foot.
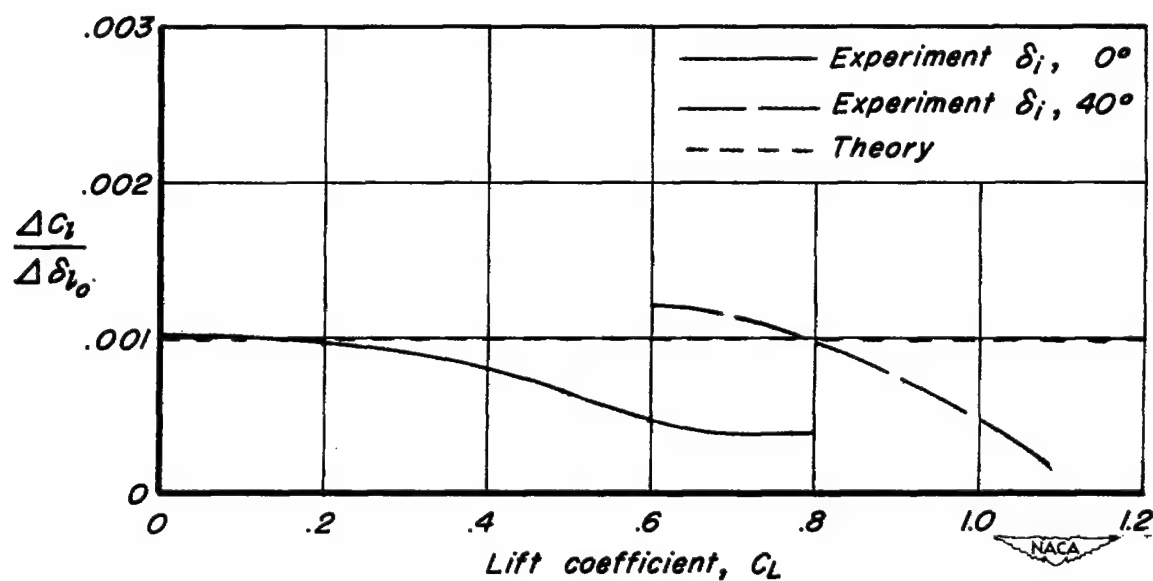
Figure 18.— Increment of rolling-moment coefficient per degree of total differential deflection of outboard flaps for the wing - fuselage — vertical-tail configuration. δ_{l_o}, 20°; δ_0, 0°.
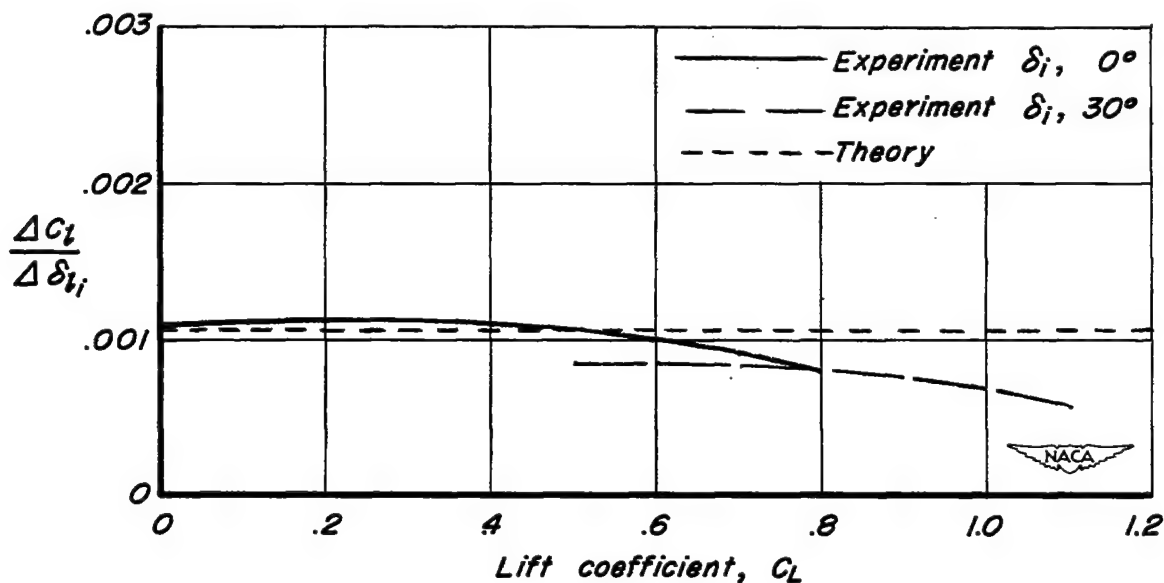
(a) Wing - fuselage — vertical - tail configuration.

Figure 19.— Increment of rolling - moment coefficient per degree
   of differential inboard – flap deflection as superposed on two
   different inboard flap settings. δ_{l_i} , 20°.
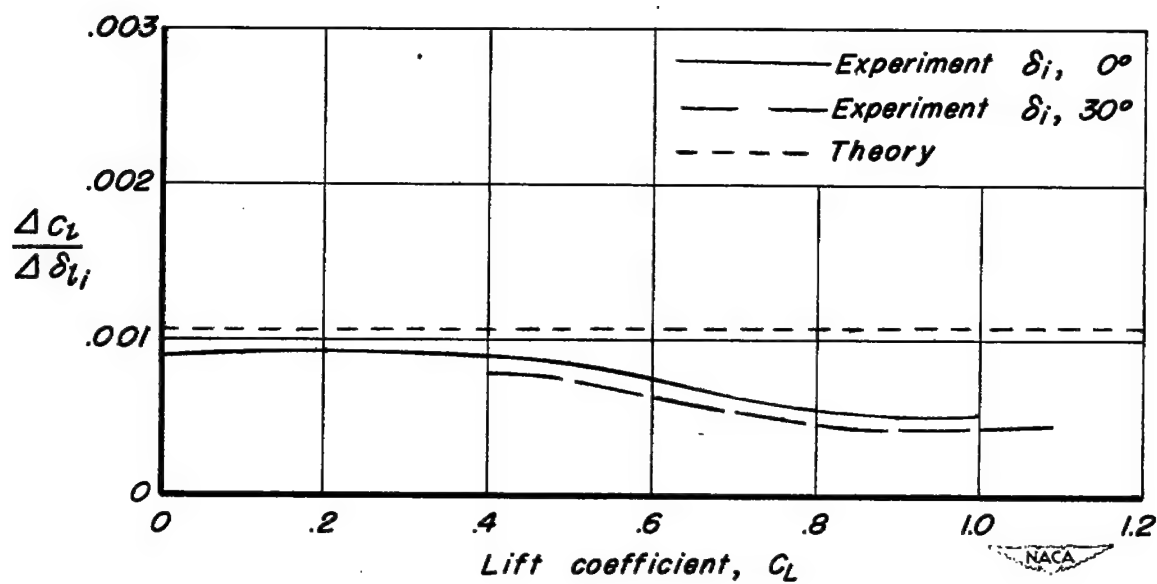
(b) Complete model. i_f, -10°.

Figure 19.— Concluded.
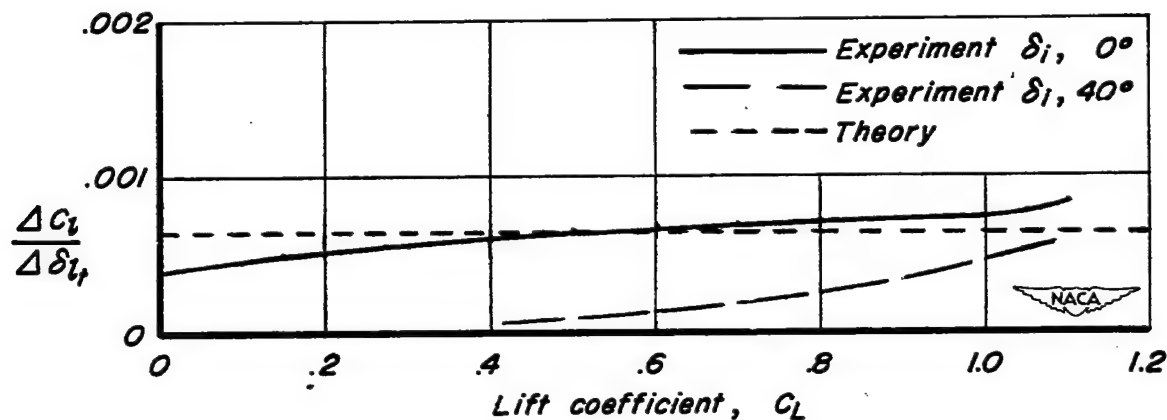
Figure 20.— Increment of rolling-moment coefficient per degree
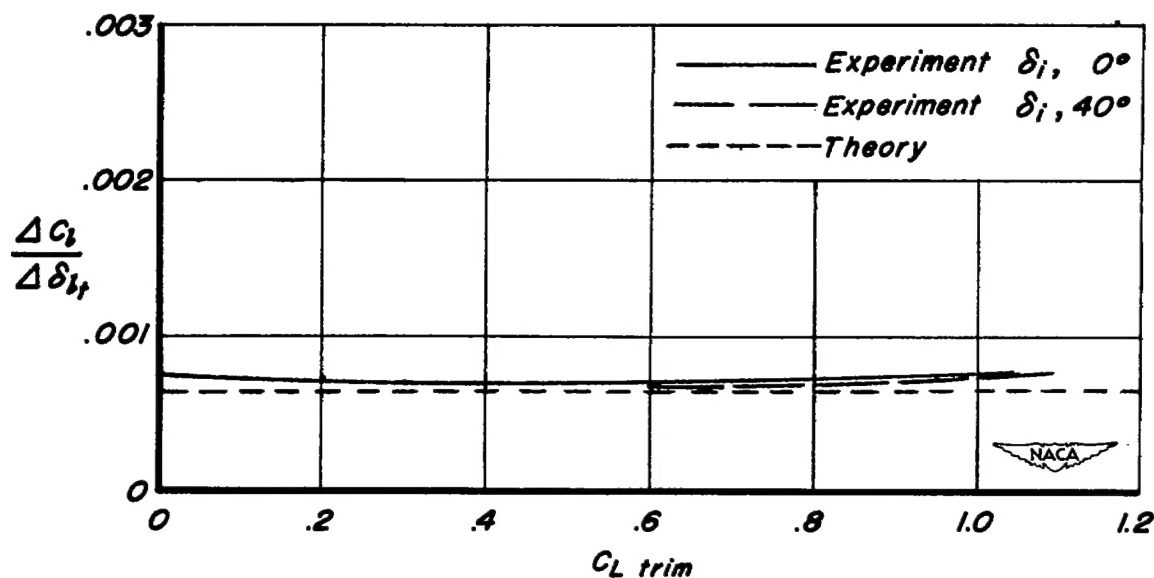of differential horizontal-tail deflection superposed on -10°
tail incidence. δ_{l_t}, 20°.

Figure 21.— Estimated increment of rolling-moment coefficient per degree of differential horizontal-tail deflection superposed on the tail deflection required for trim. δ_{i_f}, 20°.
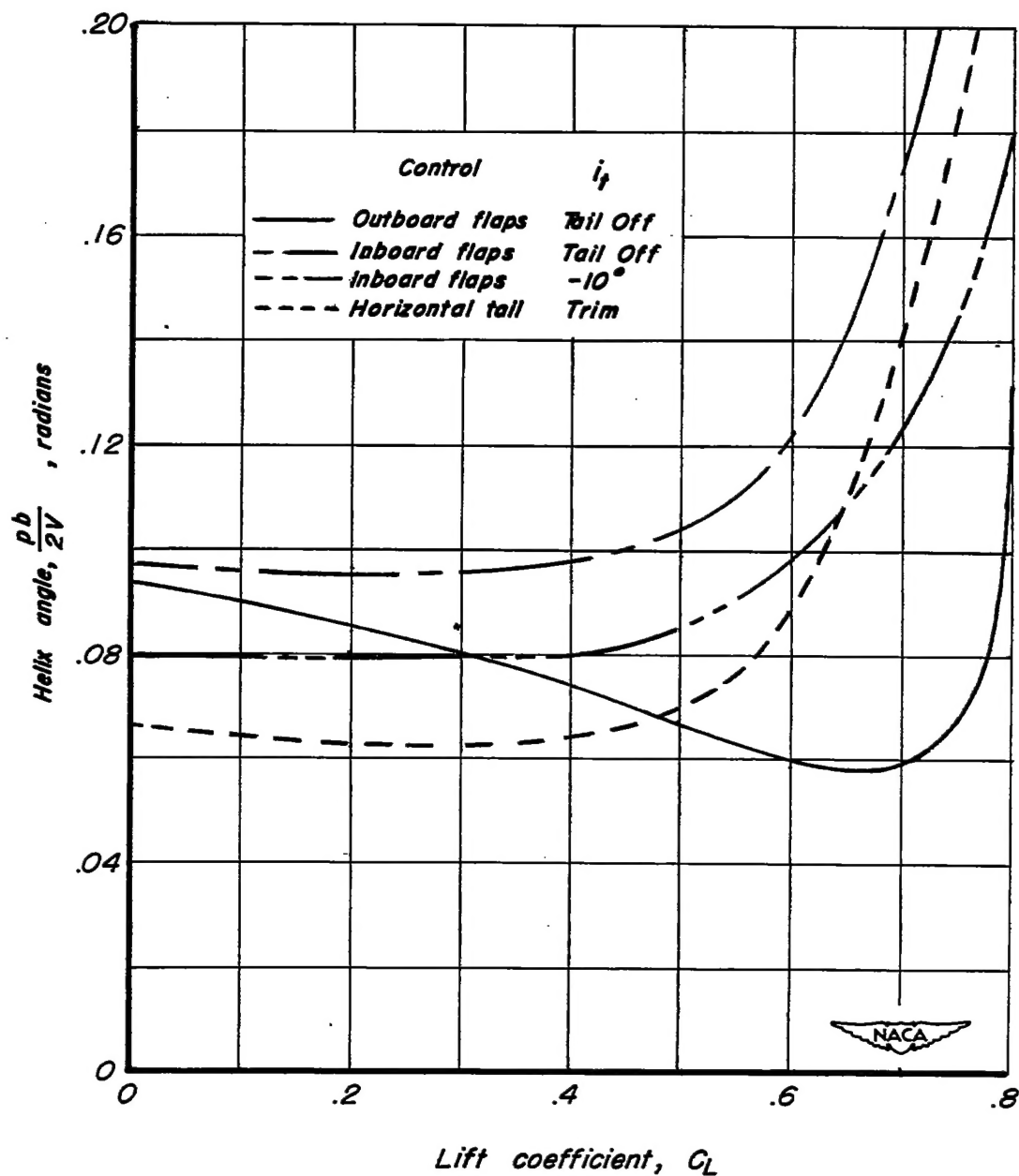
Figure 22.- Variation of wing-tip helix angle with lift coefficient for a 20° differential deflection of three types of lateral controls. δ_r, 0°; δ_i, 0°; δ_o, 0°; β, 0°.

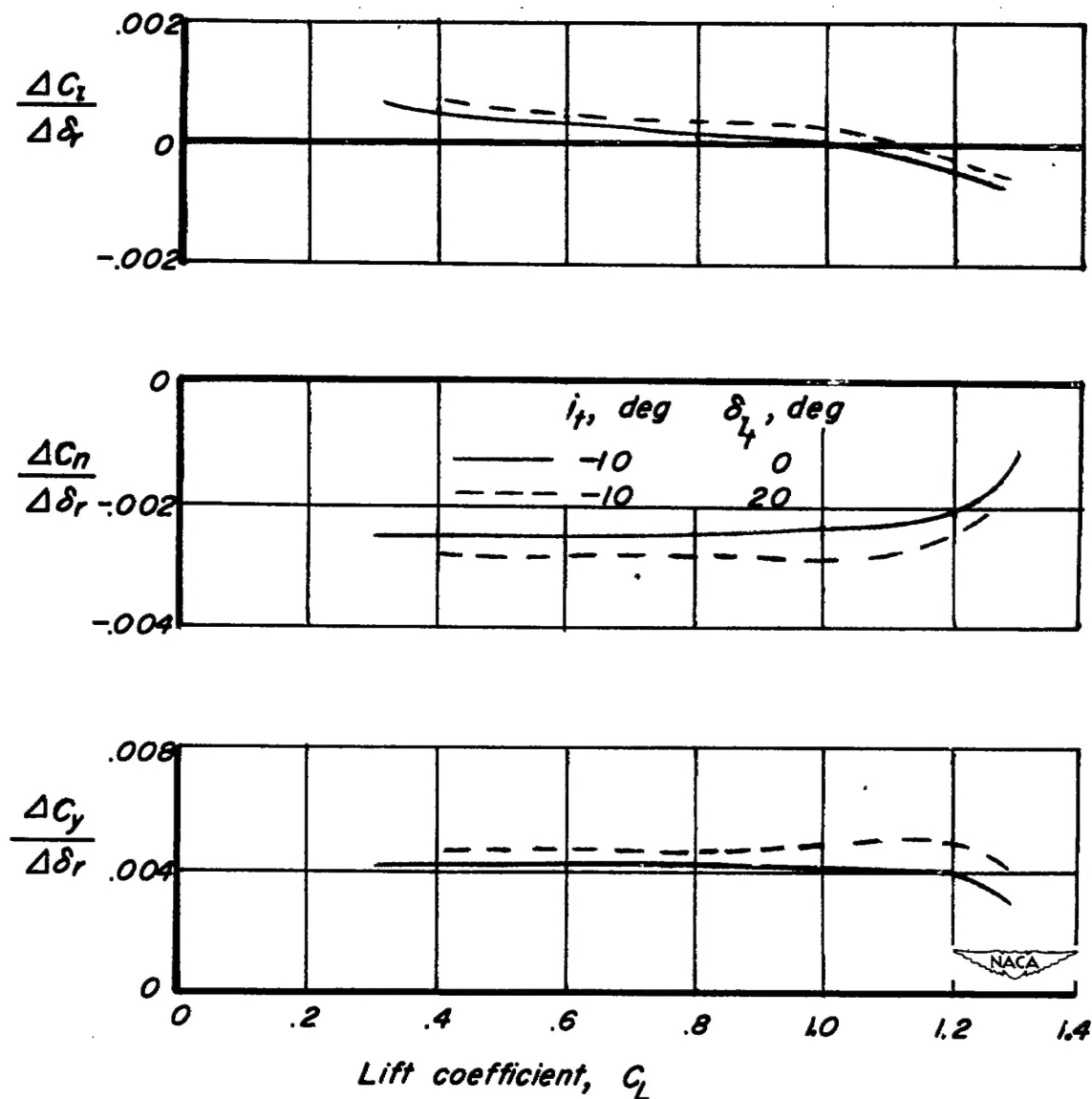Figure 23.— Effects of a differential deflection of the horizontal tail on the rudder effectiveness. δ_r, $10°$; δ_i, $40°$; β, $0°$.
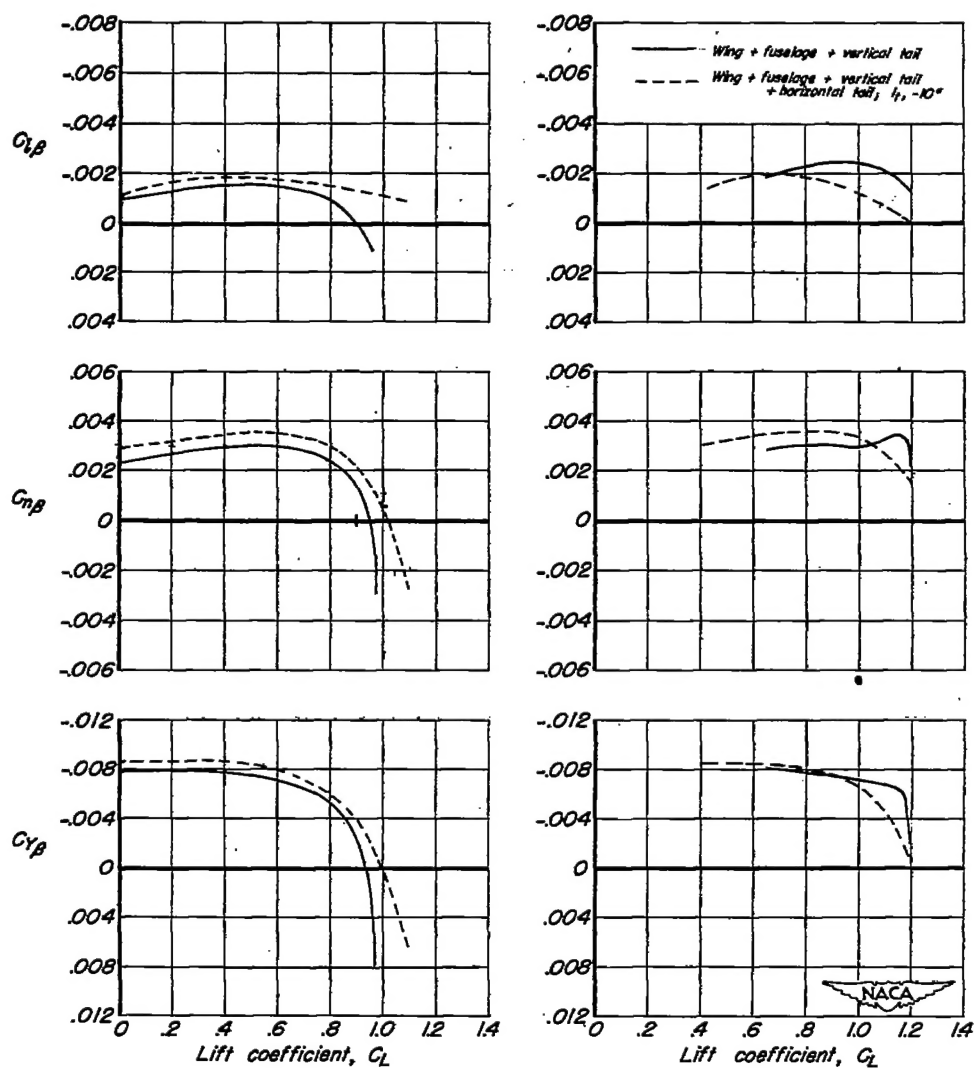
(a) δ_i, 0°   (b) δ_i, 40°

Figure 24.— Stability derivatives of the wing-fuselage — vertical-tail con-
figuration and the complete airplane model as affected by inboard-flap
deflection. δ_1, 0°; δ_o, 0°.